Article

Current Biology

Micronuclei from misaligned chromosomes that satisfy the spindle assembly checkpoint in cancer cells

Graphical abstract

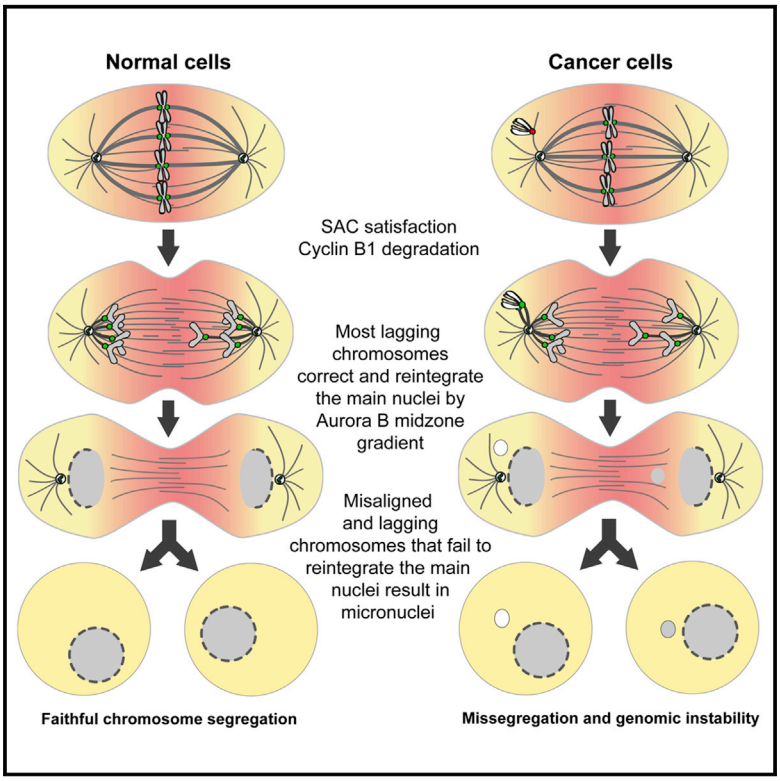

Authors

Ana Margarida Gomes, Bernardo Orr, Marco Novais-Cruz, ..., Carolina Lemos, Cristina Ferrás, Helder Maiato

Correspondence

maiato@i3s.up.pt

In brief

Gomes et al. use high-content live-cell imaging combined with RNAi to systematically investigate how human cells respond to chromosome alignment defects of distinct molecular nature. They find that misaligned chromosomes that satisfy the SAC are a strong predictor of micronuclei formation and may account for genomic instability in cancer.

Highlights

- Chromosome alignment defects of distinct molecular nature often satisfy the SAC
- Missegregation of misaligned chromosomes is a strong predictor of micronucleation
- Micronuclei formation from misaligned chromosomes is frequent in cancer cells
- Misaligned chromosomes that satisfy the SAC may drive genomic instability in cancer

Gomes et al., 2022, Current Biology *32*, 4240–4254
October 10, 2022
https://doi.org/10.1016/j.cub.2022.08.026

CellPress

CellPress
OPEN ACCESS

Current Biology

Article

Micronuclei from misaligned chromosomes that satisfy the spindle assembly checkpoint in cancer cells

Ana Margarida Gomes,[1,2,3] Bernardo Orr,[1,2,6] Marco Novais-Cruz,[1,2,3,6] Filipe De Sousa,[1,2,7] Joana Macário-Monteiro,[1,2,3] Carolina Lemos,[2,3,4] Cristina Ferrás,[1,2] and Helder Maiato[1,2,5,8,9,*]

[1]Chromosome Instability & Dynamics Group, i3S - Instituto de Investigação e Inovação em Saúde, Universidade do Porto, Rua Alfredo Allen 208, 4200-135 Porto, Portugal
[2]Instituto de Biologia Molecular e Celular, Universidade do Porto, Rua Alfredo Allen 208, 4200-135 Porto, Portugal
[3]Instituto de Ciências Biomédicas Abel Salazar, Universidade do Porto, Rua Jorge de Viterbo Ferreira 228, 4050-313 Porto, Portugal
[4]UnIGENe, i3S - Instituto de Investigação e Inovação em Saúde, Universidade do Porto, Rua Alfredo Allen 208, 4200-135 Porto, Portugal
[5]Cell Division Group, Department of Biomedicine, Faculdade de Medicina, Universidade do Porto, Alameda Prof. Hernâni Monteiro, 4200-319 Porto, Portugal
[6]These authors contributed equally
[7]Present address: Radiation Oncology Division, Geneva University Hospitals (HUG), Avenue de la Roseraie 53, 1205 Geneva, Switzerland
[8]Twitter: @mitosisrocks
[9]Lead contact
*Correspondence: maiato@i3s.up.pt
https://doi.org/10.1016/j.cub.2022.08.026

SUMMARY

Chromosome alignment to the spindle equator is a hallmark of mitosis thought to promote chromosome segregation fidelity in metazoans. Yet chromosome alignment is only indirectly supervised by the spindle assembly checkpoint (SAC) as a byproduct of chromosome bi-orientation, and the consequences of defective chromosome alignment remain unclear. Here, we investigated how human cells respond to chromosome alignment defects of distinct molecular nature by following the fate of live HeLa cells after RNAi-mediated depletion of 125 proteins previously implicated in chromosome alignment. We confirmed chromosome alignment defects upon depletion of 108/125 proteins. Surprisingly, in all confirmed cases, depleted cells frequently entered anaphase after a delay with misaligned chromosomes. Using depletion of prototype proteins resulting in defective chromosome alignment, we show that misaligned chromosomes often satisfy the SAC and directly missegregate without lagging behind in anaphase. In-depth analysis of specific molecular perturbations that prevent proper kinetochore-microtubule attachments revealed that misaligned chromosomes that missegregate frequently result in micronuclei. Higher-resolution live-cell imaging indicated that, contrary to most anaphase lagging chromosomes that correct and reintegrate the main nuclei, misaligned chromosomes are a strong predictor of micronuclei formation in a cancer cell model of chromosomal instability, but not in non-transformed near-diploid cells. We provide evidence supporting that intrinsic differences in kinetochore-microtubule attachment stability on misaligned chromosomes account for this distinct outcome. Thus, misaligned chromosomes that satisfy the SAC may represent a previously overlooked mechanism driving chromosomal/genomic instability during cancer cell division, and we unveil genetic conditions predisposing for these events.

INTRODUCTION

Chromosome alignment in human cells relies on the concerted action of motor-dependent and -independent mechanisms, which are determined by chromosome positioning at nuclear envelope breakdown (NEB), the establishment of end-on or lateral kinetochore-microtubule interactions and specific tubulin post-translational modifications.[1–8] Despite its key role in promoting mitotic fidelity,[9–11] chromosome alignment is only indirectly supervised by the spindle assembly checkpoint (SAC), which monitors the establishment of end-on kinetochore-microtubule attachments required for chromosome bi-orientation and regulates the metaphase-anaphase transition.[12,13] It is therefore widely assumed that, under physiological conditions, cells only enter anaphase once all chromosomes align and bi-orient.[14–22] However, chromosome alignment may occur independently of end-on kinetochore-microtubule attachments and chromosome bi-orientation,[5,23,24] and conditions exist in which vertebrate cells may enter anaphase in the presence of misaligned chromosomes.[25] Additionally, misaligned chromosomes generated after functional perturbation of the kinetochore-associated CENP-E/Kinesin-7 in primary mouse fibroblasts and human HeLa cells in

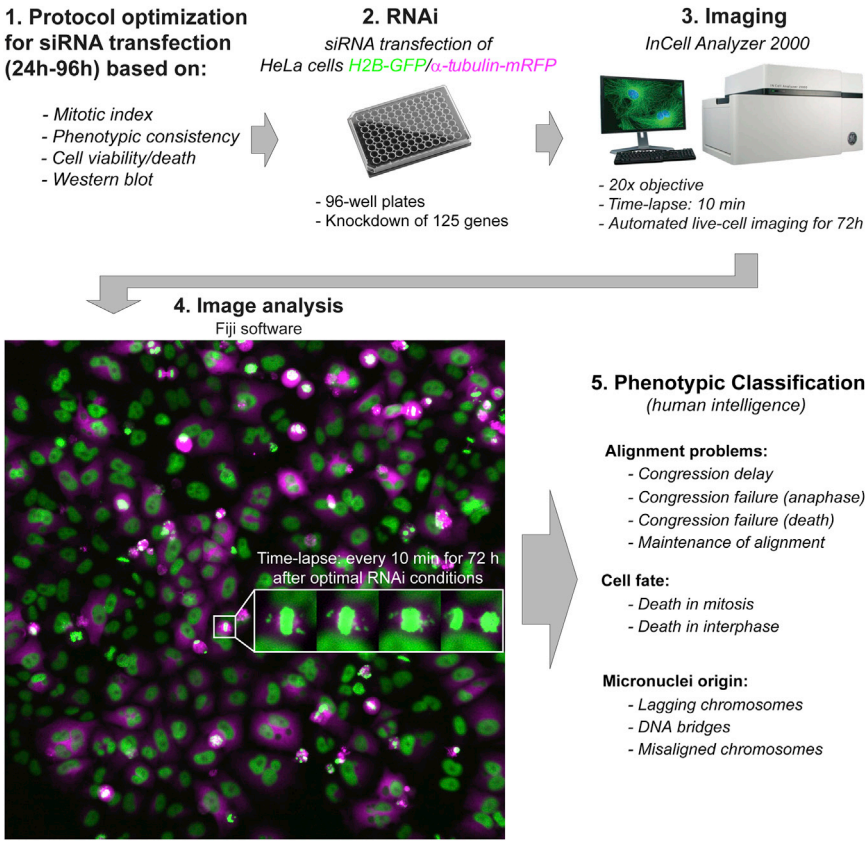

Figure 1. Schematic illustration of the high-content analysis of chromosome alignment defects

Different steps between protocol optimization and automated live-cell imaging of 125 different RNAi conditions against genes previously implicated in chromosome congression.

culture, as well as in regenerating hepatocytes *in vivo*, did not prevent anaphase onset in approximately 25%, 40%, and 95% of cell divisions, respectively, resulting in missegregation and aneuploidy.[26–28] Importantly, as opposed to massive aneuploidy that renders cells unviable and has a tumor suppressing effect,[29,30] gain/loss of just one or few chromosomes that are unable to complete alignment represents a real threat to chromosomal stability and has been shown to contribute to tumorigenesis *in vivo*.[31] Thus, understanding how human cells respond to chromosome alignment defects and determining what happens to an enduring misaligned chromosome remain fundamental unanswered questions with strong clinical implications.

RESULTS

A broad range of chromosome alignment defects directly lead to missegregation

To systematically inquire how human cells respond to chromosome alignment defects of distinct molecular nature, we used siRNAs to knockdown 125 different proteins previously implicated in this process (Data S1, S2, and S3), combined with high-content live-cell microscopy in human HeLa cells stably expressing histone H2B-GFP (to visualize chromosomes) and α-tubulin-mRFP (to visualize mitotic spindles) (Figure 1) (see also http://chromosomecongression.i3s.up.pt). Control cells underwent consecutive rounds of mitosis and completed chromosome alignment in 23 ± 8 min (mean ± SD, n = 7,229 cells), indicating no relevant phototoxicity. In contrast, experimental perturbation of chromosome alignment led to three main mitotic phenotypes: (1) cells that entered anaphase after a delay in completing chromosome alignment (≥2 SD in control-depleted cells), (2) cells that entered anaphase without completing chromosome alignment, and (3) cells that died without completing chromosome alignment (Figures 2A and 2B). In some cases (ILK, septin-7, Aki, HIP1r, ANKRD53, ASB7, NuMA, CENP-U, CEP164, CDCA4, and MCAK), we were unable to detect any significant defect in chromosome alignment under our experimental conditions (Data S1), while others (Shp2, GAK, CEP72, CEP90, CENP-H, and Mis12) turned out to be off-targets (Figure S1) and were not pursued further. Interestingly, upon depletion of several Augmin complex subunits,[32] CLASPs[33] or the Ska complex,[34] among others, a fraction of cells was also unable to maintain chromosome alignment after completing congression to the spindle equator and showed signs that resembled cohesion fatigue and/or loss of spindle pole integrity (Figures S2A and S2B). Not surprisingly, defective chromosome alignment was often associated with a significant mitotic delay, indicating a functional SAC whose timely satisfaction was nevertheless compromised (Figures 2B and S3). Moreover, the severity of the observed chromosome alignment defects varied extensively, suggesting that certain proteins, such as CENP-E, several cytoplasmic Dynein subunits, members of the KNL1, Mis12, and Ndc80 (KMN) network,[35] the Ska complex,[34] and the Augmin complex,[32] are more crucial for this process than others (Figure 2B). However, less penetrant phenotypes due to sub-optimal protein depletion cannot be excluded. Most relevant, and regardless of the underlying molecular nature, cells frequently entered anaphase with misaligned chromosomes that often missegregated.

Mild, yet penetrant, chromosome alignment defects are compatible with mitotic progression and cell viability

Next, we investigated how the extent of chromosome alignment defects impacts cell viability during and after mitosis (Figures 3A and 3B). We found a strong positive correlation between the propensity of cells to die in mitosis and the time they spent in mitosis due to chromosome alignment defects (Figures 3B–3D). A positive, yet weaker correlation was also observed between the likelihood of cells to die in the subsequent interphase and the time they spent in mitosis due to chromosome alignment defects

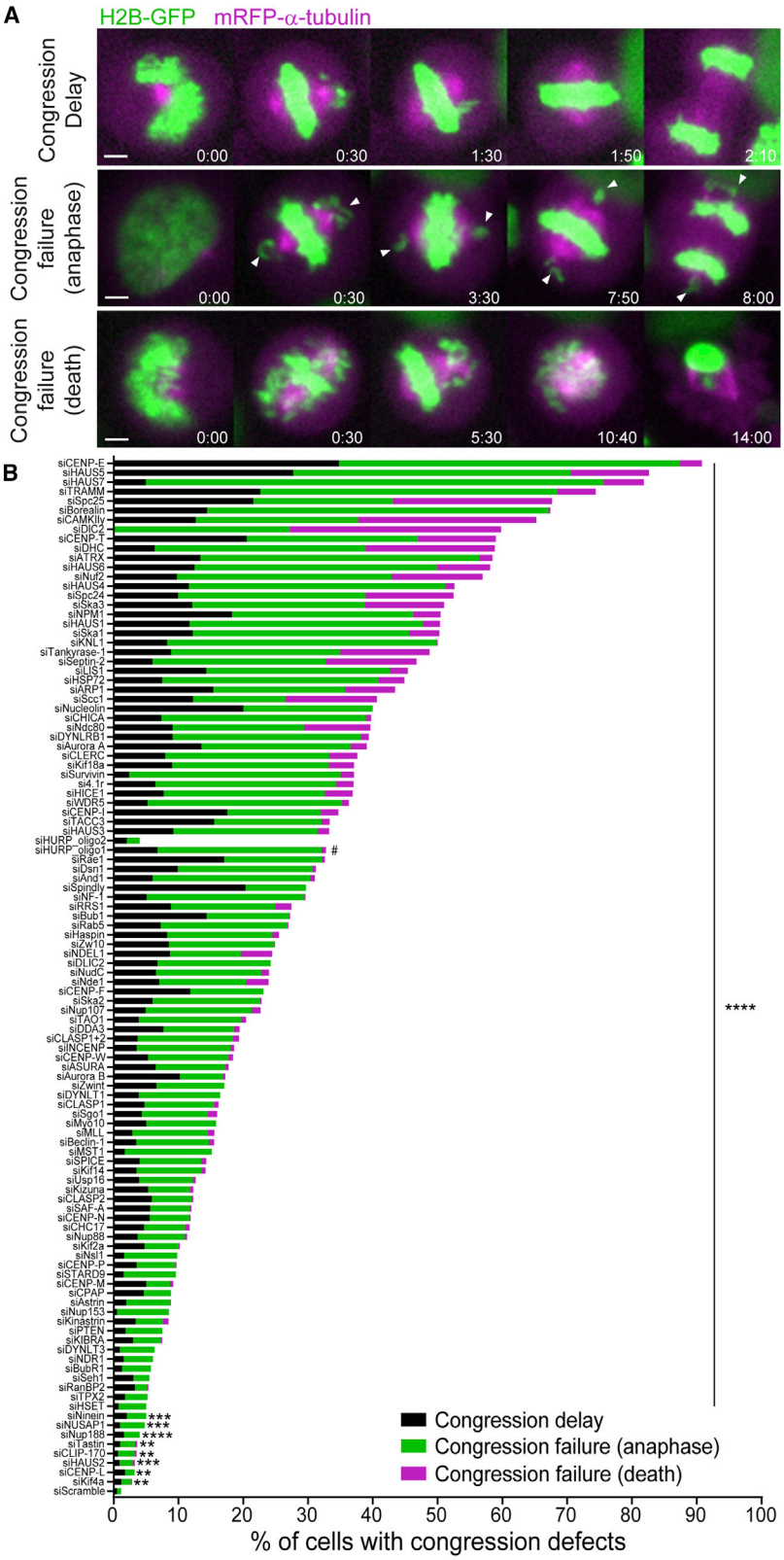

Figure 2. A broad range of chromosome alignment defects directly lead to missegregation

(A) Examples of time-lapse sequences illustrating the three main mitotic phenotypes observed. Arrows indicate chromosomes at the poles in cells exhibiting chromosome alignment defects. Pixels were saturated for optimal visualization of misaligned chromosomes. Scale bars, 5 μm. Time, h:min.

(B) Quantification of congression phenotypes in control (siScramble) and siRNA-depleted cells. At least 2 independent experiments per condition were performed.

The total number of cells analyzed for each condition is indicated in Data S1. *p ≤ 0.05, **p ≤ 0.01, ***p ≤ 0.001, ****p ≤ 0.0001; ns, not significantly different from control; Fisher's exact two-tailed test; # highlights a possible off-target associated with siRNA oligo 1 against HURP.

CellPress
OPEN ACCESS

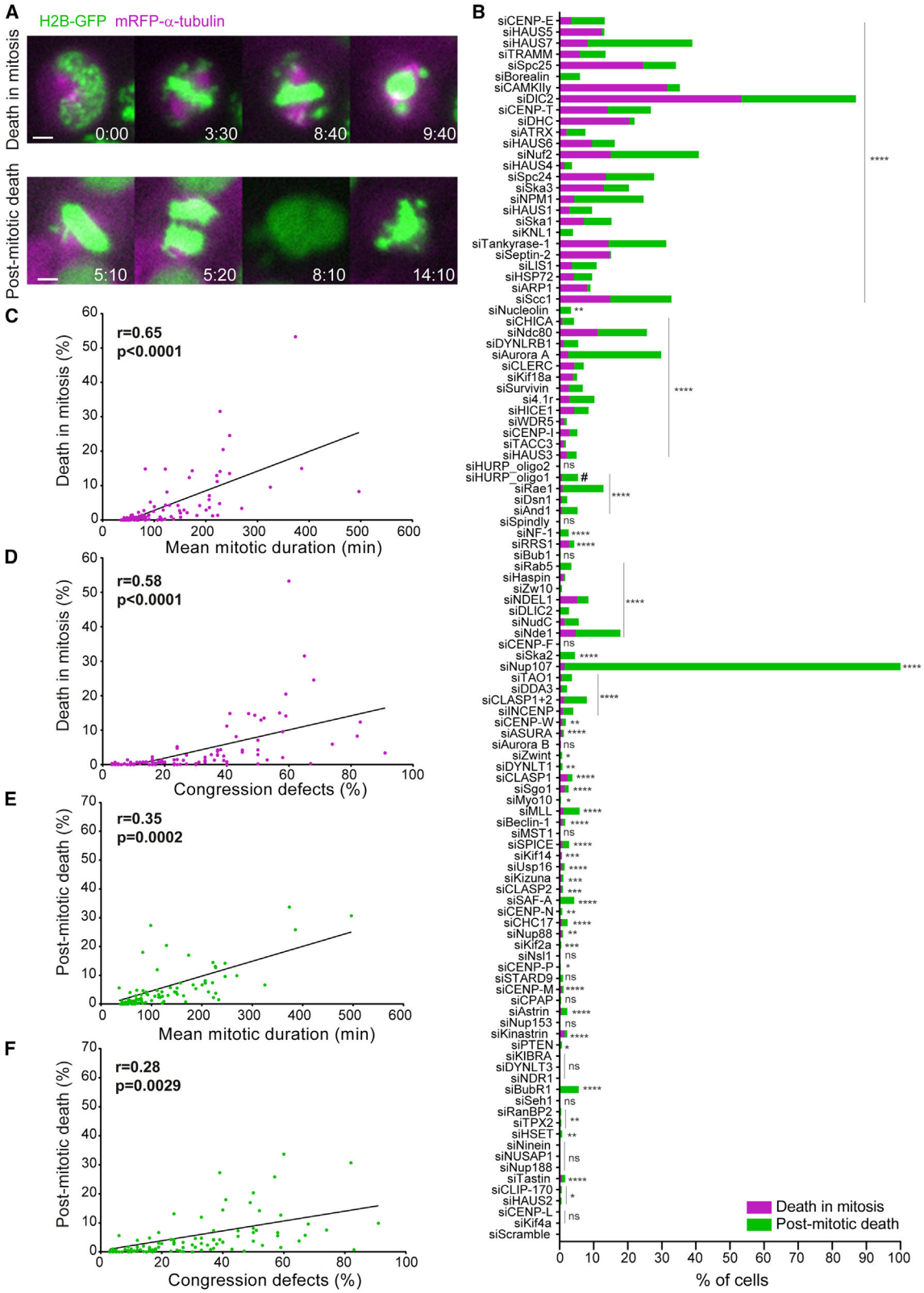

(legend on next page)

(Figures 3B, 3E, and 3F). In one particular case (NUP107 RNAi), most cells died in the subsequent interphase likely due to a well-established role in nuclear pore complex assembly and function.[36] Interestingly, a direct comparison between CENP-E-depleted (with mild, yet highly penetrant chromosome alignment problems) and Ndc80-depleted cells (with severe, but less penetrant chromosome alignment problems), revealed a clear link between the extent of chromosome alignment defects and cell death, either in mitosis or in the subsequent interphase (Figures S4A–S4B′). Importantly, conditions such as CENP-E or Kif18a depletion, in which cells entered anaphase with only one or few misaligned chromosomes, and/or a less compact metaphase plate,[10] were compatible with mitotic progression and cell viability (Figure 3B), thereby representing a threat to chromosomal stability.

Cells with misaligned chromosomes enter anaphase after satisfying the spindle assembly checkpoint

In contrast to cells that satisfy the SAC, human cells undergoing mitotic slippage[37] upon complete microtubule depolymerization with nocodazole retain the SAC proteins, Mad1, Mad2, and BubR1 at kinetochores and very slowly degrade cyclin B1 due to residual APC/C activity.[38–40] To distinguish between these possibilities, we used live imaging in HeLa cells stably expressing Mad2-GFP to monitor the status of the SAC in control- or CENP-E-depleted cells that entered anaphase with one or few misaligned chromosomes at very high frequency after a mitotic delay (Figure 2B; see also Maia et al.[27] and Tanudji et al.[28]). As expected, in cells treated with a control siRNA Mad2-GFP accumulated at kinetochores during prometaphase and gradually disappeared as chromosomes bi-oriented and aligned at the metaphase plate, being undetectable at kinetochores when cells entered anaphase (Figure 4A; Video S1). Likewise, Mad2-GFP accumulated exclusively at the kinetochores from those few chromosomes that never completed alignment after CENP-E depletion, becoming undetectable before anaphase onset and throughout anaphase (Figure 4A; Video S1). To obtain a more quantitative picture, we used immunofluorescence in fixed HeLa cells to measure the fluorescence of the SAC protein Mad1 relative to CENP-C (a constitutive kinetochore component) on misaligned chromosomes after CENP-E depletion in early anaphase (Figure 4B). We found that, in striking contrast to misaligned chromosomes during prometaphase where Mad1 signal was clearly detected at kinetochores in both control- and CENP-E-depleted cells (Figure 4C), virtually no Mad1 signal was detected at both kinetochores from misaligned chromosomes (an indication of syntelic attachments in which both kinetochores of a misaligned chromosome are oriented toward the same spindle pole) that persisted in early anaphase after CENP-E depletion (Figure 4C). Together, these data suggest that cells with misaligned chromosomes enter anaphase after a delay by satisfying the SAC.

To further validate this conclusion, we used time-lapse fluorescence microscopy in HeLa and non-transformed near-diploid RPE-1 cells to quantify the levels and monitor the respective degradation kinetics of endogenously tagged cyclin B1 with the fluorescent protein Venus[40] after depletion of CENP-E, or a second unrelated protein (TACC3) whose depletion also resulted in misaligned chromosomes[41] (Figures 2B and S5A–S5C). Consistent with previous reports[15,42] and in stark contrast with cyclin B1 degradation kinetics over more than 12 h during mitotic slippage/death upon complete microtubule depolymerization with nocodazole (Figures S5D and S5E; see also Brito and Rieder,[38] Gascoigne and Taylor,[39] and Novais-Cruz et al.[40]), cyclin B1 starts to be steadily degraded a few minutes before the onset of anaphase and continues to decline throughout anaphase in control HeLa or RPE-1 cells, becoming undetectable as chromosomes decondense in telophase (Figures 5A and 5B; Videos S2 and S3). Similar degradation kinetics were observed in CENP-E-depleted or TACC3-depleted cells that entered anaphase, with or without completion of chromosome alignment (Figures 5A, 5B, S5A, and S5B; Videos S2 and S3). In this particular set of experiments ~40% of the CENP-E-depleted and ~20% of the TACC3-depleted anaphase HeLa cells formed micronuclei directly from chromosomes that never aligned at the spindle equator and missegregated (Figure 5C). The frequency of these events was significantly lower in RPE-1 cells, likely due to higher efficiency in chromosome alignment after CENP-E depletion (Figure S5C). Taken together, these data indicate that cells with misaligned chromosomes may enter anaphase after satisfying the SAC and undergoing normal cyclin B1 degradation.

Although most micronuclei originate from anaphase lagging chromosomes, misaligned chromosomes are a stronger predictor of micronuclei formation

The origin of micronuclei has been linked to the presence of lagging chromosomes during anaphase that form due to incorrect merotelic kinetochore-microtubule attachments (when individual kinetochores bind to microtubules oriented to both spindle poles).[43,44] More recently, DNA bridges that persist during anaphase were also implicated in micronuclei formation.[45] Here, we sought to compare the relative contributions of lagging and misaligned chromosomes, as well as DNA bridges, to micronuclei formation during HeLa cell division (Figure 6A). To do so, we focused our analysis on a subset of experimental conditions that are recognized to prevent proper kinetochore-microtubule

Figure 3. Mild, yet penetrant, chromosome alignment defects are compatible with mitotic progression and cell viability

(A) Examples of time-lapse sequences illustrating the fates exhibited by HeLa cells undergoing congression defects following siRNA knockdown. Time, h:min, from nuclear envelope breakdown (NEB) to each cellular outcome. Scale bars, 5 μm.

(B) Frequency of cells that either died in mitosis (magenta) or died in interphase (green) in control and siRNA-depleted cells. The total number of cells analyzed for each condition is indicated in Data S1. *$p \leq 0.05$, **$p \leq 0.01$, ***$p \leq 0.001$, ****$p \leq 0.0001$; ns, not significantly different from control; Fisher's exact two-tailed test; # highlights a possible off-target associated with siRNA oligo 1 against HURP.

(C) Correlation between mitotic duration and cell death in mitosis for each condition.

(D) Correlation between the severity of the congression phenotypes and the frequency of cell death in mitosis.

(E) Correlation between the mitotic duration after siRNA treatment and cell death in interphase.

(F) Correlation between congression severity and the frequency of cell death in interphase. Pearson's correlation (r) and respective p values are indicated in the plots (two-tailed test).

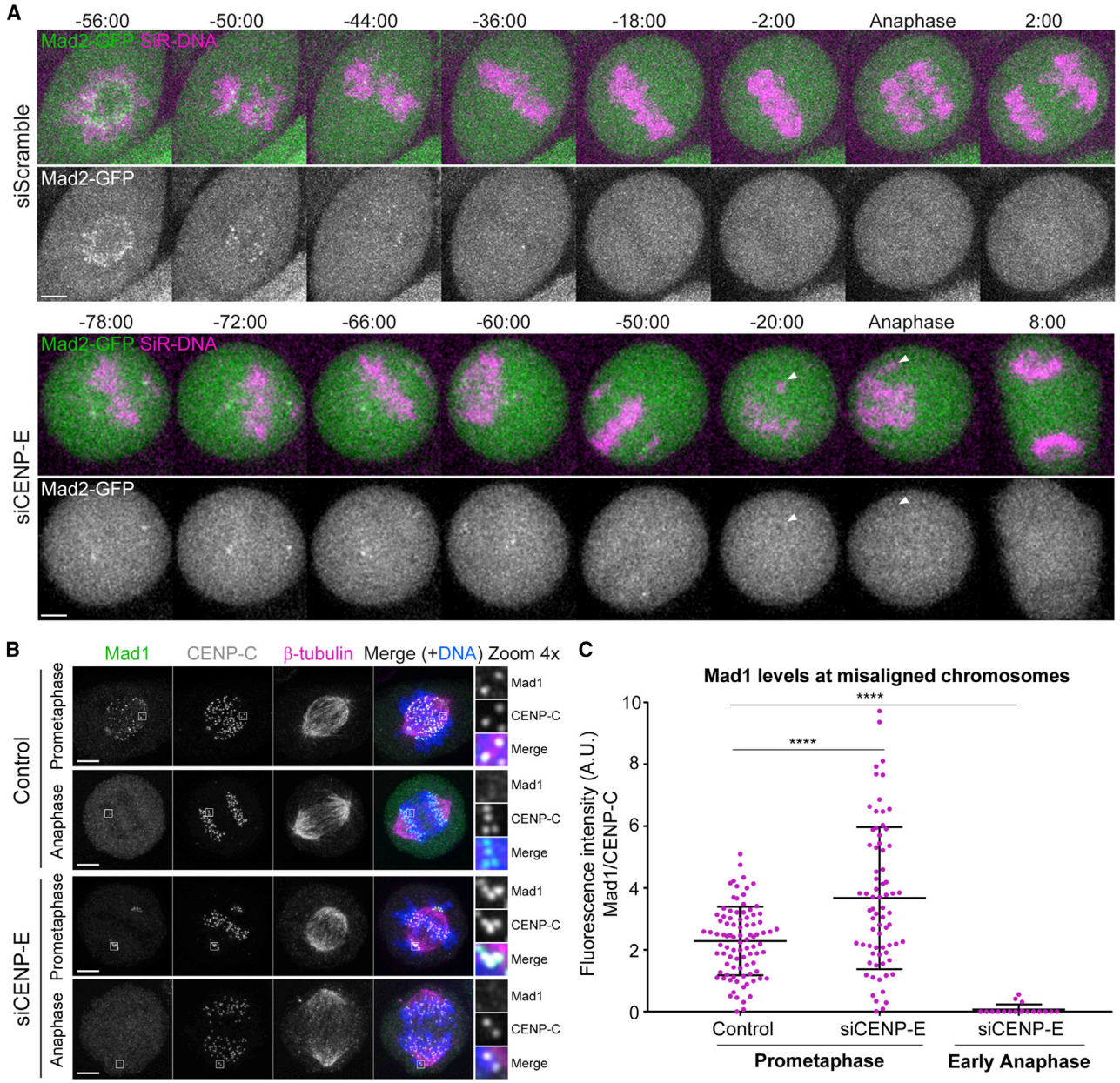

Figure 4. Cells with misaligned chromosomes enter anaphase after satisfying the spindle assembly checkpoint

(A) Selected time frames of representative HeLa cells stably expressing Mad2-GFP (green) and chromosomes labeled with SiR-DNA (magenta) in control and after CENP-E depletion. White arrowheads point to a misaligned chromosome during anaphase. Time, min:s. Time 00:00, anaphase onset.

(B) Immunofluorescence of HeLa cells stained for DNA (blue), Mad1 (green), CENP-C (white), and β-tubulin (magenta). Insets show higher magnification of selected regions with misaligned chromosomes (grayscale for single channels of Mad1 and CENP-C). Images are maximum-intensity projections of deconvolved z stacks. Scale bars, 5 μm.

(C) Quantification of the fluorescence intensity of Mad1 relative to CENP-C on misaligned chromosomes. Each dot represents an individual kinetochore. The horizontal line indicates the mean of all quantified kinetochores, and the error bars represent the standard deviation from a pool of two independent experiments (mock/prometaphase, n = 90 kinetochores, 9 cells; siCENP-E/prometaphase, n = 72 kinetochores, 17 cells; siCENP-E/anaphase, n = 19 kinetochores, 14 cells; ****$p \leq 0.0001$ relative to control, Mann-Whitney test).

attachments (Figure 6B). As a rule, and in line with our previous findings,[46] these conditions led to a substantial increase in the frequency of daughter cells with micronuclei (9.0% ± 7.3%, mean ± SD of all conditions, and up to 40% on specific conditions such as KNL1 depletion) when compared with daughter cells treated with a control siRNA (1.4%) (Figure 6B). As expected, most of the resulting micronuclei derived from anaphase lagging chromosomes (62% ± 19%, mean ± SD of all conditions) and only few (8.5% ± 6.2%, mean ± SD of all conditions) originated from DNA bridges (Figure 6B). However, we also found

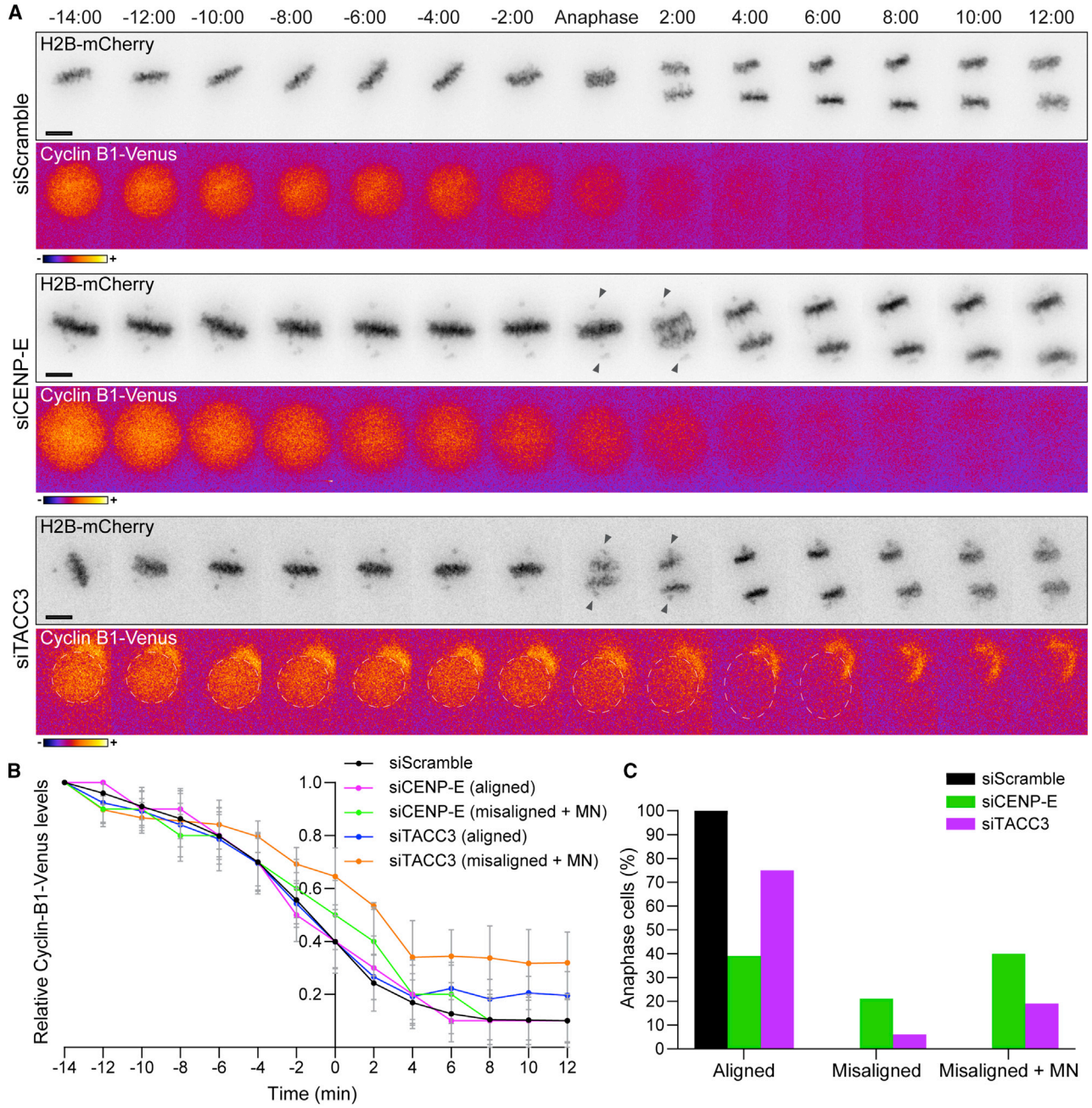

Figure 5. Cells with misaligned chromosomes enter anaphase after undergoing normal cyclin B1 degradation

(A) Selected time frames from live-cell microscopy of HeLa cells stably expressing H2B-mCherry and cyclin B1-Venus in control, CENP-E, and TACC3 RNAi. Time, min:s. Time 00:00, anaphase onset. Scale bars, 5 μm. Black arrowheads point to misaligned chromosomes at anaphase onset.

(B) Cyclin B1 degradation curves for control, CENP-E-, and TACC-3-depleted cells that properly align their chromosomes at the metaphase plate or exit mitosis with misaligned chromosomes and form micronuclei. The curves represent mean cyclin B1-Venus fluorescence intensity from all analyzed cells, and error bars represent the standard deviation from a pool of two independent experiments (siScramble n = 20; siCENP-E [misaligned + micronuclei] n = 22; siCENP-E [aligned] n = 15; siTACC3 [misaligned + micronuclei] n = 5; siTACC3 [aligned] n = 12).

(C) Frequency of anaphase cells with aligned chromosomes, misaligned chromosomes, and misaligned chromosomes that result in micronuclei in control (black bars), CENP-E- (green bars), and TACC3-depleted cells (magenta bars).

that a significant fraction of cells (29% ± 20%, mean ± SD of all conditions) formed micronuclei that derived directly from misaligned chromosomes (Figure 6B). Noteworthy, although occurring at much lower frequency, the relative origin of micronuclei in control HeLa cells was in line with that generally observed upon experimental perturbation of kinetochore-microtubule attachments (56%, 22%, and 22%, for lagging chromosomes, DNA bridges, and misaligned chromosomes, respectively;

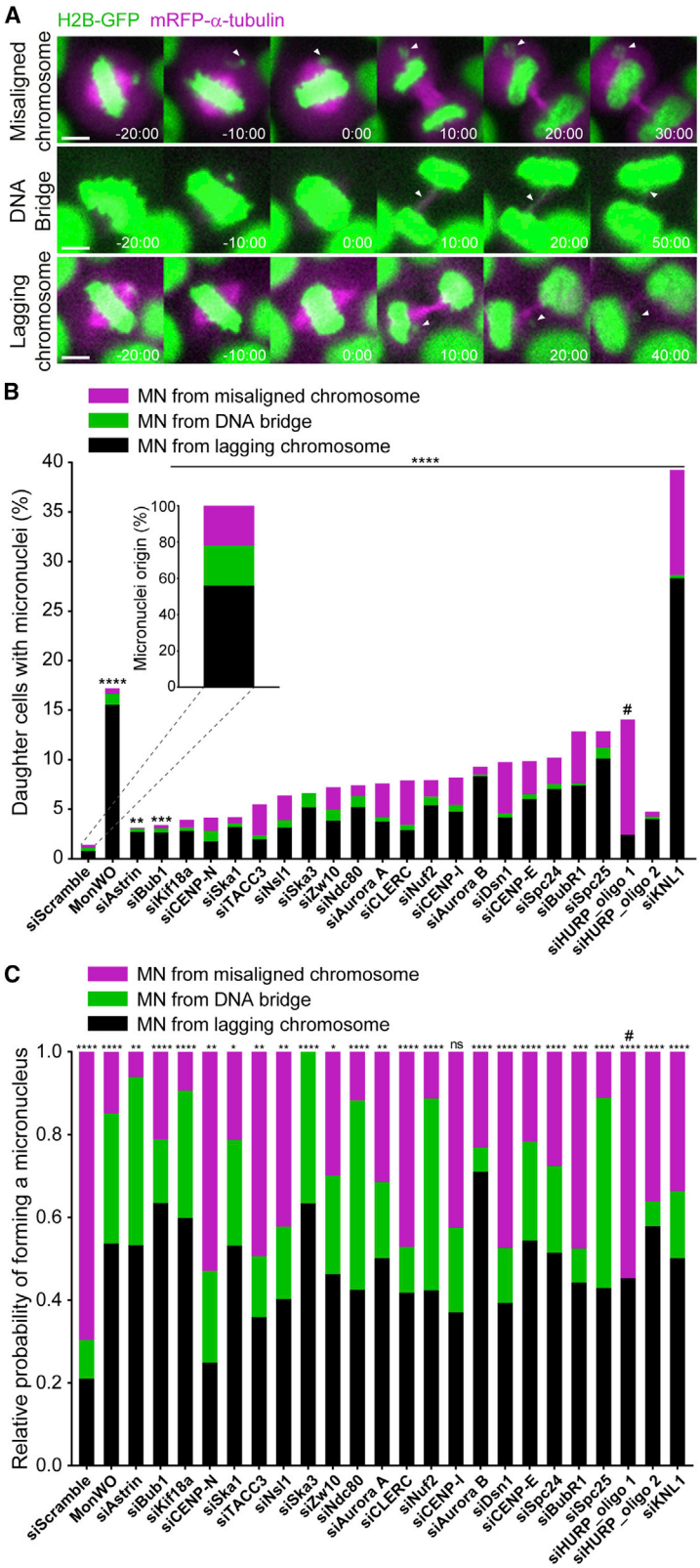

Figure 6. Although most micronuclei originate from anaphase lagging chromosomes, misaligned chromosomes are a stronger predictor of micronuclei formation

(A) Examples of time-lapse sequences illustrating the different origins of micronuclei. Time, min:s. Time 00:00, anaphase onset. White arrowheads track misaligned chromosomes, DNA bridges, or lagging chromosomes until they eventually form micronuclei. Pixels were saturated for optimal visualization of misaligned chromosomes, DNA bridges, and lagging chromosomes. Scale bars, 5 μm.

(B) Frequency of daughter cells with micronuclei that derived either from lagging chromosomes (black bars), DNA bridges (green bars), or misaligned chromosomes (magenta bars) under the specified conditions (siScramble, n = 1,700; MonWO, n = 327; siAstrin, n = 423; siBub1, n = 457; siKif18a, n = 540; siCENP-N, n = 422; siSka1, n = 395; siTACC3, n = 485; siNsl1, n = 400; siSka3, n = 383; siZw10, n = 404; siNdc80, n = 440; siAurora A, n = 388; siCLERC, n = 263; siNuf2, n = 428; siCENP-I, n = 389; siAurora B, n = 499; siDsn1, n = 688; siCENP-E, n = 346; siSpc24, n = 418; siBubR1, n = 387; siSpc25, n = 425; siHURP_oligo1, n = 296; siHURP_oligo2, n = 200; siKNL1, n = 413; pool of 2 independent experiments for each siRNAi per condition, with the exception of Aurora A and CLERC in which only 1 experiment for the second siRNAi was performed. All independent experiments were pooled). *p ≤ 0.05, **p ≤ 0.01, ***p ≤ 0.001, ****p ≤ 0.0001; ns, not significantly different from control; Fisher's exact two-tailed test; # highlight a possible off-target associated with siRNA oligo 1 against HURP.

(C) Relative probability (sum of the 3 independent absolute probabilities normalized to 1) of micronuclei formation from a lagging chromosome (black bars), a DNA bridge (green bars), or a misaligned chromosome (magenta bars) under the specified conditions (*p ≤ 0.05, **p ≤ 0.01, ***p ≤ 0.001, ****p ≤ 0.0001; ns, no significant difference from what would be expected if all missegregation events were equally likely to cause micronuclei in each experimental condition; chi-square test).

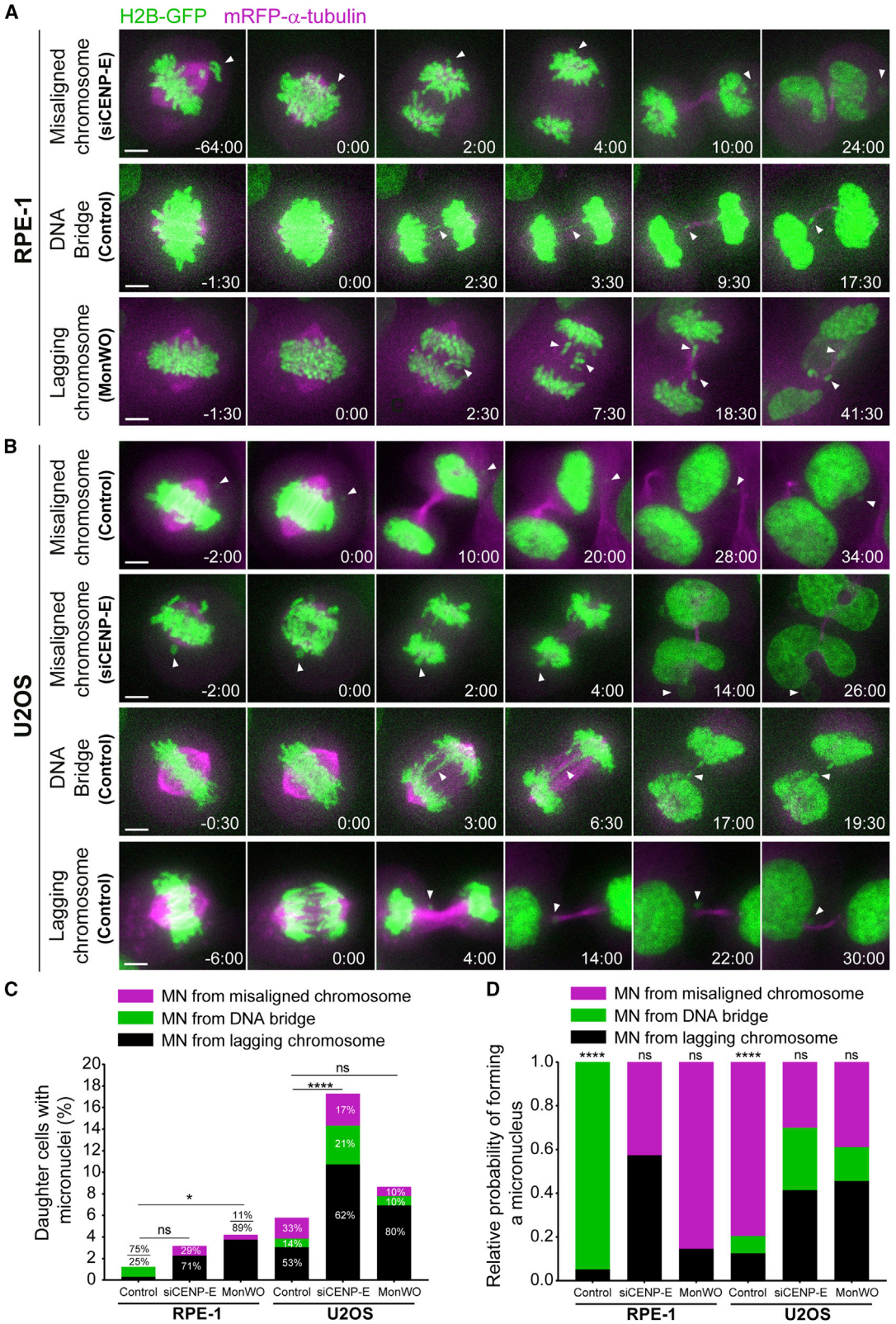

(legend on next page)

n = 1,700 cells) (Figure 6B). This scenario changed significantly both regarding frequency and origin of micronuclei upon monastrol treatment and washout, which induces the formation of erroneous kinetochore-microtubule attachments leading to a high frequency of anaphase lagging chromosomes[47,48] (Figure 6B).

Next, we determined the respective probabilities of micronuclei formation given a specific condition, which can either be a lagging chromosome, a DNA bridge, or a misaligned chromosome. Surprisingly, and despite the fact that most micronuclei derived from anaphase lagging chromosomes, we found that in unperturbed HeLa cells treated with a control siRNA the absolute and relative probability of micronuclei formation from a misaligned chromosome (0.92 and 0.70, respectively) clearly outcompeted the other two classes, including anaphase lagging chromosomes (0.28 and 0.21, for absolute and relative probabilities, respectively) (Figures 6C and S6A). Those probabilities were significantly higher than what would be expected if all missegregation events were equally likely to cause micronuclei ($p < 0.0001$; chi-square test). Interestingly, although the experimental perturbation of kinetochore-microtubule attachment stability did not result in gross alterations of the relative origins of micronuclei, in most cases, it reverted or attenuated the much higher probability of micronuclei formation from misaligned chromosomes observed in unperturbed cells (Figures 6C and S6A). This result is consistent with a role of stable kinetochore-microtubule attachments in anaphase error correction and micronuclei prevention from lagging chromosomes.[46] One noticeable exception was HURP, which gave rise to much milder congression problems with no obvious bias for micronuclei formation from misaligned chromosomes with a second siRNA, in contrast with the original siRNA, despite equivalent depletion efficiency (Data S3). We suspect that the first siRNA against HURP might by hitting the SAC component MAD2, which is highly prone to off-targeting[49] and would force HURP-depleted cells with incomplete chromosome congression to enter anaphase prematurely, directly leading to micronuclei formation due to incomplete chromosome alignment. Overall, we conclude that, although the majority of micronuclei originate from anaphase lagging chromosomes, misaligned chromosomes are a stronger predictor of micronuclei formation during HeLa cell division.

Micronuclei formation from misaligned chromosomes is a frequent outcome in a cancer cell model of chromosomal instability, but not in non-transformed near-diploid cells

Next, we set out to investigate the origin of micronuclei that form spontaneously during cell division in RPE-1 and chromosomally unstable U2OS cells.[50] To visualize the entire chromosome set and spindle microtubules, these cell lines were engineered to stably express histone H2B-GFP and mRFP-α-tubulin and were inspected by 4D live-cell spinning-disk confocal microscopy, with a temporal resolution between 30 s and 2 min (Figures 7A and 7B). In parallel, we promoted chromosome missegregation by performing either CENP-E depletion or a monastrol treatment and washout. Unperturbed RPE-1 cells showed only a residual (1.2%) formation of micronuclei after cell division and none derived from a misaligned chromosome (Figure 7C). CENP-E depletion or monastrol treatment/washout in RPE-1 cells significantly increased the frequency of micronuclei formation (3.2% and 4.2%, respectively), most of which (71% and 89%, respectively) derived from anaphase lagging chromosomes, and only very few derived from a misaligned chromosome (2.1% and 0.95% of the cells, respectively) (Figure 7C), further demonstrating a robust chromosome alignment capacity in normal cells. This scenario was strikingly different even in unperturbed U2OS cells, which formed micronuclei in 5.8% of the cases, of which 53% derived from anaphase lagging chromosomes, 14% from DNA bridges and 33% from misaligned chromosomes (Figure 7C). Monastrol treatment/washout only slightly increased (without statistical significance) the percentage of dividing U2OS cells that formed micronuclei, which in this case derived mostly from anaphase lagging chromosomes (80%), likely due to an increase in merotelic attachments.[47] In contrast, CENP-E depletion in U2OS cells significantly increased the percentage of dividing U2OS cells that formed micronuclei (17.2%), of which 62% derived from anaphase lagging chromosomes, 21% from DNA bridges and 17% from misaligned chromosomes (Figure 7C).

We next determined the relative probabilities of micronuclei formation from lagging chromosomes, DNA bridges, and misaligned chromosomes scored in both RPE-1 and U2OS cells, with and without CENP-E, as well as with and without monastrol treatment/washout (Figure 7D) (for absolute probabilities, see Figure S6B). In line with our previous observations in HeLa cells (Figures 6C and S6A), this analysis revealed that misaligned chromosomes have the highest absolute and relative probability of resulting in micronuclei in unperturbed chromosomally unstable U2OS cells (0.63 and 0.80, respectively) (Figures 7D and S6B). These probabilities were significantly higher than what would be expected if all missegregation events were equally likely to cause micronuclei ($p < 0.0001$; chi-square test). In agreement with our findings in HeLa cells, both CENP-E depletion and monastrol treatment/washout reverted this tendency in U2OS

Figure 7. Micronuclei formation from misaligned chromosomes is a frequent outcome in a chromosomally unstable cancer cell model, but not in non-transformed cells

(A and B) Examples of time-lapse sequences illustrating possible origins of micronuclei in RPE-1 (A) and U2OS (B) cells. Time, min:s. Time 00:00, anaphase onset. White arrowheads track misaligned chromosomes, DNA bridges, or lagging chromosomes until they eventually form micronuclei. Pixels were saturated for optimal visualization of misaligned chromosomes, DNA bridges, and lagging chromosomes. Scale bars, 5 μm.

(C) Frequency of RPE-1 and U2OS daughter cells with micronuclei that derived either from lagging chromosomes (black bars), DNA bridges (green bars), or misaligned chromosomes (magenta bars) in control, siCENP-E, and after monastrol treatment/washout (MonWO). RPE-1 cells: control, n = 163; siCENP-E, n = 95; MonWO, n = 105. U2OS cells: control, n = 250; siCENP-E, n = 81; MonWO, n = 49 (Fisher's exact two-tailed test).

(D) Relative probability (sum of the 3 independent absolute probabilities normalized to 1) of micronuclei formation from a lagging chromosome (black bars), a DNA bridge (green bars), or a misaligned chromosome (magenta bars) in RPE-1 and U2OS cells in control and after CENP-E depletion or monastrol treatment/washout. *$p \leq 0.05$, **$p \leq 0.01$, ***$p \leq 0.001$, ****$p \leq 0.0001$; ns, no significant difference from what would be expected if all missegregation events were equally likely to cause micronuclei in each experimental condition; chi-square test.

cells, likely due to a significant increase in the frequency of anaphase lagging chromosomes (Figures 7C, 7D, and S6B).[47] Most striking, and in sharp contrast to unperturbed HeLa and U2OS cells, unperturbed RPE-1 cells always entered anaphase after completing chromosome alignment and, consequently, no micronuclei from misaligned chromosomes were ever detected in our recordings (Figures 7D and S6B). Likewise, human primary fibroblasts were previously shown to never enter anaphase with misaligned chromosomes even after nocodazole treatment and washout, and the resulting lagging chromosomes appeared during anaphase after completing chromosome alignment during metaphase.[44] We concluded that spontaneous misaligned chromosomes in unperturbed chromosomally unstable cancer cell models, but not in non-transformed near-diploid cells, have a strong probability to missegregate and result in micronuclei.

Misaligned chromosomes in chromosomally unstable cancer cells have hyper-stabilized kinetochore-microtubule attachments

Chromosomally unstable cancer cells have hyper-stabilized kinetochore-microtubule attachments and a poor error correction capacity.[50,51] To investigate whether increased kinetochore-microtubule attachment stability in chromosomally unstable cancer cells allows misaligned chromosomes to satisfy the SAC, we implemented a protocol that promotes the formation of few misaligned chromosomes after nocodazole treatment and washout (Figure S7A) (STAR Methods), followed by quantification of fluorescence intensity after a nocodazole shock to completely depolymerize microtubules in fixed cells (Figure S7A). Both qualitative and quantitative analyses revealed that, under these experimental conditions, kinetochore microtubules in chromosomally unstable U2OS cells are more resistant to depolymerization when compared with non-transformed near-diploid RPE-1 cells (Figures S7A and S7B). Measurement of the respective half-life of polymerized tubulin, confirmed ~2-fold increase in U2OS cells relative to RPE1 cells (Figures S7A and S7B). These results provide an explanation for the inefficient correction of few misaligned chromosomes that eventually satisfy the SAC in a chromosomally unstable cancer cell model and thus may represent important drivers of chromosomal instability and micronuclei formation in human cancers.

DISCUSSION

It is currently thought that anaphase lagging chromosomes resulting from erroneous merotelic attachments that satisfy the SAC are major drivers of genomic instability in human cancers.[52,53] Although anaphase lagging chromosomes resulting from merotelic attachments rarely missegregate,[54,55] they may fail to incorporate into the respective daughter nuclei during cell division and result in the formation of micronuclei. Micronuclei were recently implicated as key intermediates of chromothripsis, a series of massive genomic rearrangements that may drive rapid tumor evolution and account for acquired drug resistance and oncogene activation.[43,56–59] We now show that although most micronuclei derive from anaphase lagging chromosomes, simply because these events occur at a very high frequency in chromosomally unstable cancer cells,[54] misaligned chromosomes that satisfy the SAC often directly missegregate (without lagging behind in anaphase) and have the highest probability to form micronuclei, specifically in human cancer cell models (see graphical abstract). This is consistent with recent high-resolution live-cell studies in both cancer and non-cancer human cells that showed that the vast majority of lagging chromosomes have a transient nature and are corrected during anaphase by an Aurora-B-dependent mechanism that prevents micronuclei formation,[46,60] and the relatively low frequency of micronuclei formation even after induction of massive chromosome segregation errors by experimental abrogation of the SAC.[61,62]

Defects in chromosome alignment are normally avoided by increased Aurora B activity at centromeres of misaligned chromosomes.[27] However, the correction of erroneous attachments underlying some chromosome alignment defects (e.g., syntelic attachments) appears to be less robust in cancer cells that also show overly stabilized kinetochore-microtubule attachments.[50,51] Indeed, RPE-1 cells treated with microtubule-targeting drugs at concentrations that stabilize microtubules satisfy the SAC in the presence of misaligned chromosomes and do so faster under conditions that promote the formation of syntelic attachments.[62–64] In addition to direct missegregation from misaligned chromosomes, late-aligning chromosomes are also more prone to lag behind in anaphase and missegregate at higher frequencies in human cancer cells, or upon SAC inactivation or stabilization of incorrect kinetochore-microtubule attachments in normal cells.[62,65] Together with the fact that non-transformed human cells rely on a robust p53-dependent mechanism that limits the proliferation of aneuploid cells,[66] the present work helps to explain how spontaneous misaligned chromosomes in cancer cells eventually satisfy the SAC and may constitute a direct route to chromosomal instability.

This work also unveils a wide range of genetic perturbations that predispose for these events and might account for the underlying chromosomal and genomic instability commonly observed in human cancers. A paramount case is the perturbation of CENP-E function that has been linked to tumorigenesis *in vivo*.[31] Previous studies have shown that ~40% of CENP-E-depleted HeLa cells enter anaphase with misaligned chromosomes.[27,28] Fixed-cell analysis revealed that these misaligned chromosomes accumulate Mad2, but micronuclei generated from CENP-E-depleted cells did not, suggesting that misaligned chromosomes satisfy the SAC.[27] Although suggestive, the origin of the scored micronuclei was not determined in these fixed-cell experiments, and so it remains possible that the scored micronuclei did not derive directly from misaligned chromosomes (they may alternatively derive from anaphase lagging chromosomes; Figures 6B and 6C), and cells with misaligned chromosomes entered anaphase without satisfying the SAC. Indeed, previous experiments in fixed CENP-E KO MEFs revealed continued localization of SAC proteins at misaligned chromosomes seen in anaphase cells, suggesting ongoing SAC signaling.[26] Our live-cell imaging of Mad2-GFP upon CENP-E depletion in HeLa cells, supported by quantitative analyses in fixed cells soon after anaphase onset, show that Mad1/Mad2 dissociate from kinetochores of misaligned chromosomes in cells that entered anaphase, suggesting SAC satisfaction. Moreover, live-cell imaging revealed a normal

degradation kinetics of cyclin B1 in CENP-E-depleted or unrelated TACC3-depleted cells that entered anaphase with misaligned chromosomes. This contrasts with the pattern observed upon mitotic slippage, in which mitotic cells that cannot satisfy the SAC exit mitosis with high Mad1/Mad2 levels at kinetochores and after very slow and prolonged degradation of cyclin B1.[39,64,67] Combined, these data provide direct evidence that, at least under certain conditions, cancer cells with misaligned chromosomes may enter anaphase after SAC satisfaction and have a high risk of forming micronuclei (see graphical abstract). In line with these findings, recent experiments in which CENP-E activity was inhibited in human RPE-1 cells suggest that endomembrane "ensheathing" of misaligned chromosomes may facilitate micronuclei formation and delay SAC satisfaction.[68]

Our systematic analysis of more than 100 different molecular perturbations further indicates that entering anaphase with misaligned chromosomes might be a frequent outcome in cancer cells. In particular, perturbations such as CENP-E or Kif18a depletion were largely compatible with cell viability, despite the high incidence of cells that entered anaphase in the presence of misaligned chromosomes. This contrasts with more drastic scenarios that result from perturbation of end-on kinetochore-microtubule attachments (e.g., depletion of KMN components) that often result in massive chromosome missegregation and cell death. Noteworthy, while the loss of Kif18a, which causes asynchronous segregation of misaligned chromosomes due to loss of interchromosome compaction during anaphase, does not promote chromosomal instability and tumorigenesis,[10,69] the loss of CENP-E that typically originates one or few pole-proximal chromosomes directly leads to aneuploidy and the spontaneous formation of lymphomas and lung tumors in aged animals.[26,31] These data suggest that the origin and properties of the resulting micronuclei is genetically determined and might have implications for the propensity to undergo massive chromosome rearrangements, such as those commonly observed in chromothripsis. Interestingly, micronuclei derived from segregation errors associated with Kif18a loss of function appear to form stable nuclear envelopes.[69] However, because misaligned chromosomes that form after perturbation of CENP-E function are brought very close to Aurora A activity at the spindle poles,[2] this might compromise proper nuclear envelope formation.[70,71] In agreement, micronuclei derived from misaligned chromosomes after CENP-E perturbation were recently suggested to activate the cGAS-STING pathway in cancer cells.[72] Thus, cellular response to micronuclei might depend on their relative origin. Overall, our findings incite for an in-depth characterization of the properties and fate of micronuclei of different origins, while evaluating their respective potential to drive and/or sustain cell transformation. In this regard, our study indicates that micronuclei formation from misaligned chromosomes appears to be a specific outcome of cancer cells and may represent a possible therapeutic opportunity in human cancers.

STAR★METHODS

Detailed methods are provided in the online version of this paper and include the following:

SUPPLEMENTAL INFORMATION

Supplemental information can be found online at https://doi.org/10.1016/j.cub.2022.08.026.

ACKNOWLEDGMENTS

We thank André Maia for technical assistance. A.M.G., M.N.-C., and J.M.-M. are recipients of PhD studentships from Fundação para a Ciência e a Tecnologia (FCT) (SFRH/BD/130938/2017, SFRH/BD/117063/2016, and 2021.07945.BD). This work was funded by the European Research Council consolidator grant CODECHECK, under the European Union's Horizon 2020 research and innovation program (681443), FCT (PTDC/MED-ONC/3479/2020), and a La Caixa Health Research Grant (LCF/PR/HR21/52410025).

AUTHOR CONTRIBUTIONS

Conceptualization, supervision, project administration, and funding acquisition, H.M.; methodology, A.M.G., B.O., M.N.-C., F.D.S., and C.F.; investigation, formal analysis, and validation, A.M.G., B.O., M.N.-C., F.D.S., C.F., J.M.-M., C.L., and H.M.; visualization, A.M.G., B.O., M.N.-C., F.D.S., C.F., J.M.-M., and H.M.; writing – original draft, A.M.G. and H.M.; writing – review & editing, A.M.G., B.O., M.N.-C., C.F., and H.M.

DECLARATION OF INTERESTS

B.O. declares that he is a consultant specialist at Volastra Therapeutics.

Received: February 14, 2022
Revised: July 22, 2022
Accepted: August 11, 2022
Published: September 2, 2022

REFERENCES

1. Maiato, H., Gomes, A.M., Sousa, F., and Barisic, M. (2017). Mechanisms of chromosome congression during mitosis. Biology *6*, 13. https://doi.org/10.3390/biology6010013.
2. Barisic, M., Aguiar, P., Geley, S., and Maiato, H. (2014). Kinetochore motors drive congression of peripheral polar chromosomes by overcoming random arm-ejection forces. Nat. Cell Biol. *16*, 1249–1256. https://doi.org/10.1038/ncb3060.
3. Yang, Z., Tulu, U.S., Wadsworth, P., and Rieder, C.L. (2007). Kinetochore dynein is required for chromosome motion and congression independent of the spindle checkpoint. Curr. Biol. *17*, 973–980.

4. Vorozhko, V.V., Emanuele, M.J., Kallio, M.J., Stukenberg, P.T., and Gorbsky, G.J. (2008). Multiple mechanisms of chromosome movement in vertebrate cells mediated through the Ndc80 complex and dynein/dynactin. Chromosoma *117*, 169–179.
5. Kapoor, T.M., Lampson, M.A., Hergert, P., Cameron, L., Cimini, D., Salmon, E.D., McEwen, B.F., and Khodjakov, A. (2006). Chromosomes can congress to the metaphase plate before biorientation. Science *311*, 388–391. https://doi.org/10.1126/science.1122142.
6. Wood, K.W., Sakowicz, R., Goldstein, L.S., and Cleveland, D.W. (1997). CENP-E is a plus end-directed kinetochore motor required for metaphase chromosome alignment. Cell *91*, 357–366.
7. Barisic, M., Silva e Sousa, R., Tripathy, S.K., Magiera, M.M., Zaytsev, A.V., Pereira, A.L., Janke, C., Grishchuk, E.L., and Maiato, H. (2015). Mitosis. Microtubule detyrosination guides chromosomes during mitosis. Science *348*, 799–803. https://doi.org/10.1126/science.aaa5175.
8. Barisic, M., and Maiato, H. (2016). The tubulin code: a navigation system for chromosomes during mitosis. Trends Cell Biol. *26*, 766–775. https://doi.org/10.1016/j.tcb.2016.06.001.
9. Orr, B., and Maiato, H. (2019). No chromosome left behind: the importance of metaphase alignment for mitotic fidelity. J. Cell Biol. *218*, 1086–1088. https://doi.org/10.1083/jcb.201902041.
10. Fonseca, C.L., Malaby, H.L.H., Sepaniac, L.A., Martin, W., Byers, C., Czechanski, A., Messinger, D., Tang, M., Ohi, R., Reinholdt, L.G., et al. (2019). Mitotic chromosome alignment ensures mitotic fidelity by promoting interchromosomal compaction during anaphase. J. Cell Biol. *218*, 1148–1163. https://doi.org/10.1083/jcb.201807228.
11. Matos, I., Pereira, A.J., Lince-Faria, M., Cameron, L.A., Salmon, E.D., and Maiato, H. (2009). Synchronizing chromosome segregation by flux-dependent force equalization at kinetochores. J. Cell Biol. *186*, 11–26. https://doi.org/10.1083/jcb.200904153.
12. Lara-Gonzalez, P., Pines, J., and Desai, A. (2021). Spindle assembly checkpoint activation and silencing at kinetochores. Semin. Cell Dev. Biol. *117*, 86–98. https://doi.org/10.1016/j.semcdb.2021.06.009.
13. Rieder, C.L., Schultz, A., Cole, R., and Sluder, G. (1994). Anaphase onset in vertebrate somatic cells is controlled by a checkpoint that monitors sister kinetochore attachment to the spindle. J. Cell Biol. *127*, 1301–1310.
14. Taylor, S.S., and McKeon, F. (1997). Kinetochore localization of murine Bub1 is required for normal mitotic timing and checkpoint response to spindle damage. Cell *89*, 727–735. https://doi.org/10.1016/s0092-8674(00)80255-x.
15. Clute, P., and Pines, J. (1999). Temporal and spatial control of cyclin B1 destruction in metaphase. Nat. Cell Biol. *1*, 82–87. https://doi.org/10.1038/10049.
16. Howell, B.J., Hoffman, D.B., Fang, G., Murray, A.W., and Salmon, E.D. (2000). Visualization of Mad2 dynamics at kinetochores, along spindle fibers, and at spindle poles in living cells. J. Cell Biol. *150*, 1233–1250. https://doi.org/10.1083/jcb.150.6.1233.
17. Maresca, T.J., and Salmon, E.D. (2009). Intrakinetochore stretch is associated with changes in kinetochore phosphorylation and spindle assembly checkpoint activity. J. Cell Biol. *184*, 373–381. https://doi.org/10.1083/jcb.200808130.
18. Murray, A.W. (2011). A brief history of error. Nat. Cell Biol. *13*, 1178–1182. https://doi.org/10.1038/ncb2348.
19. Pesenti, M.E., Weir, J.R., and Musacchio, A. (2016). Progress in the structural and functional characterization of kinetochores. Curr. Opin. Struct. Biol. *37*, 152–163. https://doi.org/10.1016/j.sbi.2016.03.003.
20. Acquaviva, C., Herzog, F., Kraft, C., and Pines, J. (2004). The anaphase promoting complex/cyclosome is recruited to centromeres by the spindle assembly checkpoint. Nat. Cell Biol. *6*, 892–898. https://doi.org/10.1038/ncb1167.
21. Pereira, A.J., and Maiato, H. (2012). Maturation of the kinetochore-microtubule interface and the meaning of metaphase. Chromosome Res. *20*, 563–577. https://doi.org/10.1007/s10577-012-9298-8.
22. Hein, J.B., and Nilsson, J. (2014). Stable MCC binding to the APC/C is required for a functional spindle assembly checkpoint. EMBO Rep. *15*, 264–272. https://doi.org/10.1002/embr.201337496.
23. Cai, S., O'Connell, C.B., Khodjakov, A., and Walczak, C.E. (2009). Chromosome congression in the absence of kinetochore fibres. Nat. Cell Biol. *11*, 832–838. https://doi.org/10.1038/ncb1890.
24. Khodjakov, A., Cole, R.W., McEwen, B.F., Buttle, K.F., and Rieder, C.L. (1997). Chromosome fragments possessing only one kinetochore can congress to the spindle equator. J. Cell Biol. *136*, 229–240.
25. Rieder, C.L., Davison, E.A., Jensen, L.C., Cassimeris, L., and Salmon, E.D. (1986). Oscillatory movements of monooriented chromosomes and their position relative to the spindle pole result from the ejection properties of the aster and half-spindle. J. Cell Biol. *103*, 581–591.
26. Weaver, B.A., Bonday, Z.Q., Putkey, F.R., Kops, G.J., Silk, A.D., and Cleveland, D.W. (2003). Centromere-associated protein-E is essential for the mammalian mitotic checkpoint to prevent aneuploidy due to single chromosome loss. J. Cell Biol. *162*, 551–563. https://doi.org/10.1083/jcb.200303167.
27. Maia, A.F., Feijão, T., Vromans, M.J., Sunkel, C.E., and Lens, S.M. (2010). Aurora B kinase cooperates with CENP-E to promote timely anaphase onset. Chromosoma *119*, 405–413. https://doi.org/10.1007/s00412-010-0265-x.
28. Tanudji, M., Shoemaker, J., L'Italien, L., Russell, L., Chin, G., and Schebye, X.M. (2004). Gene silencing of CENP-E by small interfering RNA in HeLa cells leads to missegregation of chromosomes after a mitotic delay. Mol. Biol. Cell *15*, 3771–3781. https://doi.org/10.1091/mbc.e03-07-0482.
29. Kops, G.J., Foltz, D.R., and Cleveland, D.W. (2004). Lethality to human cancer cells through massive chromosome loss by inhibition of the mitotic checkpoint. Proc. Natl. Acad. Sci. USA *101*, 8699–8704. https://doi.org/10.1073/pnas.0401142101.
30. Silk, A.D., Zasadil, L.M., Holland, A.J., Vitre, B., Cleveland, D.W., and Weaver, B.A. (2013). Chromosome missegregation rate predicts whether aneuploidy will promote or suppress tumors. Proc. Natl. Acad. Sci. USA *110*, E4134–E4141. https://doi.org/10.1073/pnas.1317042110.
31. Weaver, B.A., Silk, A.D., Montagna, C., Verdier-Pinard, P., and Cleveland, D.W. (2007). Aneuploidy acts both oncogenically and as a tumor suppressor. Cancer Cell *11*, 25–36. https://doi.org/10.1016/j.ccr.2006.12.003.
32. Uehara, R., Nozawa, R.-S., Tomioka, A., Petry, S., Vale, R.D., Obuse, C., and Goshima, G. (2009). The augmin complex plays a critical role in spindle microtubule generation for mitotic progression and cytokinesis in human cells. Proc. Natl. Acad. Sci. USA *106*, 6998–7003. https://doi.org/10.1073/pnas.0901587106.
33. Logarinho, E., Maffini, S., Barisic, M., Marques, A., Toso, A., Meraldi, P., and Maiato, H. (2012). CLASPs prevent irreversible multipolarity by ensuring spindle-pole resistance to traction forces during chromosome alignment. Nat. Cell Biol. *14*, 295–303. https://doi.org/10.1038/ncb2423.
34. Gaitanos, T.N., Santamaria, A., Jeyaprakash, A.A., Wang, B., Conti, E., and Nigg, E.A. (2009). Stable kinetochore-microtubule interactions depend on the Ska complex and its new component Ska3/C13Orf3. EMBO J. *28*, 1442–1452. https://doi.org/10.1038/emboj.2009.96.
35. Cheeseman, I.M., Chappie, J.S., Wilson-Kubalek, E.M., and Desai, A. (2006). The conserved KMN network constitutes the core microtubule-binding site of the kinetochore. Cell *127*, 983–997. https://doi.org/10.1016/j.cell.2006.09.039.
36. Beck, M., and Hurt, E. (2017). The nuclear pore complex: understanding its function through structural insight. Nat. Rev. Mol. Cell Biol. *18*, 73–89. https://doi.org/10.1038/nrm.2016.147.
37. Rieder, C.L., and Maiato, H. (2004). Stuck in division or passing through: what happens when cells cannot satisfy the spindle assembly checkpoint. Dev. Cell *7*, 637–651. https://doi.org/10.1016/j.devcel.2004.09.002.

38. Brito, D.A., and Rieder, C.L. (2006). Mitotic checkpoint slippage in humans occurs via cyclin B destruction in the presence of an active checkpoint. Curr. Biol. *16*, 1194–1200. https://doi.org/10.1016/j.cub.2006.04.043.

39. Gascoigne, K.E., and Taylor, S.S. (2008). Cancer cells display profound intra- and interline variation following prolonged exposure to antimitotic drugs. Cancer Cell *14*, 111–122. https://doi.org/10.1016/j.ccr.2008.07.002.

40. Novais-Cruz, M., Alba Abad, M., van IJcken, W.F., Galjart, N., Jeyaprakash, A.A., Maiato, H., and Ferrás, C. (2018). Mitotic progression, arrest, exit or death relies on centromere structural integrity, rather than de novo transcription. eLife *7*, e36898. https://doi.org/10.7554/eLife.36898.

41. Gergely, F., Draviam, V.M., and Raff, J.W. (2003). The ch-TOG/XMAP215 protein is essential for spindle pole organization in human somatic cells. Genes Dev. *17*, 336–341. https://doi.org/10.1101/gad.245603.

42. Afonso, O., Castellani, C.M., Cheeseman, L.P., Ferreira, J.G., Orr, B., Ferreira, L.T., Chambers, J.J., Morais-de-Sá, E., Maresca, T.J., and Maiato, H. (2019). Spatiotemporal control of mitotic exit during anaphase by an aurora B-Cdk1 crosstalk. eLife *8*, e47646. https://doi.org/10.7554/eLife.47646.

43. Crasta, K., Ganem, N.J., Dagher, R., Lantermann, A.B., Ivanova, E.V., Pan, Y., Nezi, L., Protopopov, A., Chowdhury, D., and Pellman, D. (2012). DNA breaks and chromosome pulverization from errors in mitosis. Nature *482*, 53–58. https://doi.org/10.1038/nature10802.

44. Cimini, D., Fioravanti, D., Salmon, E.D., and Degrassi, F. (2002). Merotelic kinetochore orientation versus chromosome mono-orientation in the origin of lagging chromosomes in human primary cells. J. Cell Sci. *115*, 507–515.

45. Umbreit, N.T., Zhang, C.Z., Lynch, L.D., Blaine, L.J., Cheng, A.M., Tourdot, R., Sun, L., Almubarak, H.F., Judge, K., Mitchell, T.J., et al. (2020). Mechanisms generating cancer genome complexity from a single cell division error. Science *368*, eaba0712. https://doi.org/10.1126/science.aba0712.

46. Orr, B., De Sousa, F., Gomes, A.M., Afonso, O., Ferreira, L.T., Figueiredo, A.C., and Maiato, H. (2021). An anaphase surveillance mechanism prevents micronuclei formation from frequent chromosome segregation errors. Cell Rep. *37*, 109783. https://doi.org/10.1016/j.celrep.2021.109783.

47. Cimini, D., Moree, B., Canman, J.C., and Salmon, E.D. (2003). Merotelic kinetochore orientation occurs frequently during early mitosis in mammalian tissue cells and error correction is achieved by two different mechanisms. J. Cell Sci. *116*, 4213–4225. https://doi.org/10.1242/jcs.00716.

48. Lampson, M.A., Renduchitala, K., Khodjakov, A., and Kapoor, T.M. (2004). Correcting improper chromosome-spindle attachments during cell division. Nat. Cell Biol. *6*, 232–237. https://doi.org/10.1038/ncb1102.

49. Sigoillot, F.D., Lyman, S., Huckins, J.F., Adamson, B., Chung, E., Quattrochi, B., and King, R.W. (2012). A bioinformatics method identifies prominent off-targeted transcripts in RNAi screens. Nat. Methods *9*, 363–366. https://doi.org/10.1038/nmeth.1898.

50. Bakhoum, S.F., Genovese, G., and Compton, D.A. (2009). Deviant kinetochore microtubule dynamics underlie chromosomal instability. Curr. Biol. *19*, 1937–1942. https://doi.org/10.1016/j.cub.2009.09.055.

51. Salimian, K.J., Ballister, E.R., Smoak, E.M., Wood, S., Panchenko, T., Lampson, M.A., and Black, B.E. (2011). Feedback control in sensing chromosome biorientation by the aurora B kinase. Curr. Biol. *21*, 1158–1165. https://doi.org/10.1016/j.cub.2011.06.015.

52. Bakhoum, S.F., and Cantley, L.C. (2018). The multifaceted role of chromosomal instability in cancer and its microenvironment. Cell *174*, 1347–1360. https://doi.org/10.1016/j.cell.2018.08.027.

53. Soto, M., Raaijmakers, J.A., and Medema, R.H. (2019). Consequences of genomic diversification induced by segregation errors. Trends Genet. *35*, 279–291. https://doi.org/10.1016/j.tig.2019.01.003.

54. Thompson, S.L., and Compton, D.A. (2011). Chromosome missegregation in human cells arises through specific types of kinetochore-microtubule attachment errors. Proc. Natl. Acad. Sci. USA *108*, 17974–17978. https://doi.org/10.1073/pnas.1109720108.

55. Cimini, D., Cameron, L.A., and Salmon, E.D. (2004). Anaphase spindle mechanics prevent mis-segregation of merotelically oriented chromosomes. Curr. Biol. *14*, 2149–2155. https://doi.org/10.1016/j.cub.2004.11.029.

56. Zhang, C.Z., Spektor, A., Cornils, H., Francis, J.M., Jackson, E.K., Liu, S., Meyerson, M., and Pellman, D. (2015). Chromothripsis from DNA damage in micronuclei. Nature *522*, 179–184. https://doi.org/10.1038/nature14493.

57. Shoshani, O., Brunner, S.F., Yaeger, R., Ly, P., Nechemia-Arbely, Y., Kim, D.H., Fang, R., Castillon, G.A., Yu, M., Li, J.S.Z., et al. (2021). Chromothripsis drives the evolution of gene amplification in cancer. Nature *591*, 137–141. https://doi.org/10.1038/s41586-020-03064-z.

58. Stephens, P.J., Greenman, C.D., Fu, B., Yang, F., Bignell, G.R., Mudie, L.J., Pleasance, E.D., Lau, K.W., Beare, D., Stebbings, L.A., et al. (2011). Massive genomic rearrangement acquired in a single catastrophic event during cancer development. Cell *144*, 27–40. https://doi.org/10.1016/j.cell.2010.11.055.

59. Janssen, A., van der Burg, M., Szuhai, K., Kops, G.J., and Medema, R.H. (2011). Chromosome segregation errors as a cause of DNA damage and structural chromosome aberrations. Science *333*, 1895–1898. https://doi.org/10.1126/science.1210214.

60. Sen, O., Harrison, J.U., Burroughs, N.J., and McAinsh, A.D. (2021). Kinetochore life histories reveal the origins of chromosome mis-segregation and correction mechanisms. Preprint at bioRxiv. https://doi.org/10.1101/2021.03.30.436326.

61. Cohen-Sharir, Y., McFarland, J.M., Abdusamad, M., Marquis, C., Bernhard, S.V., Kazachkova, M., Tang, H., Ippolito, M.R., Laue, K., Zerbib, J., et al. (2021). Aneuploidy renders cancer cells vulnerable to mitotic checkpoint inhibition. Nature *590*, 486–491. https://doi.org/10.1038/s41586-020-03114-6.

62. Klaasen, S.J., Truong, M.A., van Jaarsveld, R.H., Koprivec, I., Štimac, V., de Vries, S.G., Risteski, P., Kodba, S., Vukušić, K., de Luca, K.L., et al. (2022). Nuclear chromosome locations dictate segregation error frequencies. Nature *607*, 604–609. https://doi.org/10.1038/s41586-022-04938-0.

63. Yang, Z., Kenny, A.E., Brito, D.A., and Rieder, C.L. (2009). Cells satisfy the mitotic checkpoint in Taxol, and do so faster in concentrations that stabilize syntelic attachments. J. Cell Biol. *186*, 675–684. https://doi.org/10.1083/jcb.200906150.

64. Brito, D.A., Yang, Z., and Rieder, C.L. (2008). Microtubules do not promote mitotic slippage when the spindle assembly checkpoint cannot be satisfied. J. Cell Biol. *182*, 623–629. https://doi.org/10.1083/jcb.200805072.

65. Kuniyasu, K., Iemura, K., and Tanaka, K. (2018). Delayed chromosome alignment to the spindle equator increases the rate of chromosome missegregation in cancer cell lines. Biomolecules *9*, 10. https://doi.org/10.3390/biom9010010.

66. Thompson, S.L., and Compton, D.A. (2010). Proliferation of aneuploid human cells is limited by a p53-dependent mechanism. J. Cell Biol. *188*, 369–381. https://doi.org/10.1083/jcb.200905057.

67. Canman, J.C., Sharma, N., Straight, A., Shannon, K.B., Fang, G., and Salmon, E.D. (2002). Anaphase onset does not require the microtubule-dependent depletion of kinetochore and centromere-binding proteins. J. Cell Sci. *115*, 3787–3795. https://doi.org/10.1242/jcs.00057.

68. Ferrandiz, N., Downie, L., Starling, G.P., and Royle, S.J. (2021). Endomembranes promote chromosome missegregation by ensheathing misaligned chromosomes. Preprint at bioRxiv. https://doi.org/10.1101/2021.04.23.441091.

69. Sepaniac, L.A., Martin, W., Dionne, L.A., Stearns, T.M., Reinholdt, L.G., and Stumpff, J. (2021). Micronuclei in Kif18a mutant mice form stable micronuclear envelopes and do not promote tumorigenesis. J. Cell Biol. *220*, e202101165. https://doi.org/10.1083/jcb.202101165.

70. Portier, N., Audhya, A., Maddox, P.S., Green, R.A., Dammermann, A., Desai, A., and Oegema, K. (2007). A microtubule-independent role for

centrosomes and aurora a in nuclear envelope breakdown. Dev. Cell *12*, 515–529. https://doi.org/10.1016/j.devcel.2007.01.019.

71. Hachet, V., Canard, C., and Gönczy, P. (2007). Centrosomes promote timely mitotic entry in C. elegans embryos. Dev. Cell *12*, 531–541. https://doi.org/10.1016/j.devcel.2007.02.015.

72. Hakozaki, Y., Kashima, Y., Morita, T.Y., Tanaka, K., Kobayashi, S.S., and Ohashi, A. (2021). Abstract 1030: CENP-E inhibition generates micronucleus formation activating the cGAS-STING pathway in cancer cells. Cancer Res. *81*, 1030. https://doi.org/10.1158/1538-7445.AM2021-1030.

73. Maffini, S., Maia, A.R.R., Manning, A.L., Maliga, Z., Pereira, A.L., Junqueira, M., et al. (2009). Motor-independent targeting of CLASPs to kinetochores by CENP-E promotes microtubule turnover and poleward flux. Curr. Biol. *19*, 1566–1572.

74. Schweizer, N., Ferrás, C., Kern, D.M., Logarinho, E., Cheeseman, I.M., and Maiato, H. (2013). Spindle assembly checkpoint robustness requires Tpr-mediated regulation of Mad1/Mad2 proteostasis. J. Cell Biol. *203*, 883–893. https://doi.org/10.1083/jcb.201309076.

STAR★METHODS

KEY RESOURCES TABLE

REAGENT or RESOURCE	SOURCE	IDENTIFIER
Antibodies		
mouse anti-Mad1	Merck Millipore	Cat#MABE867; RRID:AB_2910099
mouse anti-α-tubulin	Sigma	T5168; RRID:AB_477579
rabbit anti-β-tubulin	Abcam	Ab6046; RRID:AB_2210370
guinea pig anti-CENP-C	MBL International	PD030; RRID:AB_10693556
mouse anti-Aim1	BD Biosciences	Cat#611083; RRID:AB_398396
mouse anti-Hec1 (9GA)	Abcam	Ab3613; RRID:AB_303949
mouse anti-Dsn1	Gift from A. Musacchio	N/A
mouse anti-ATRX	Santa Cruz Biotechnology	sc-55584; RRID:AB_831012
rabbit anti-CEP72	Novus Biologicals	NB100-60661; RRID:AB_920952
mouse anti-GAK	R&D Systems	MAB6918; RRID:AB_10972463
rabbit anti-WDHD1/And-1	Novus Biologicals	NBP1-89091; RRID:AB_11041095
rabbit anti-Aurora A	Novus Biologicals	NB100-267; RRID:AB_10002481
rabbit anti-HURP	Gift from P. Meraldi	N/A
mouse anti-INCENP	Santa Cruz Biotechnology	sc-376514; RRID:AB_11149761
mouse anti-Sgo1 (F-8)	Santa Cruz Biotechnology	sc-393993; RRID:AB_2910101
rabbit anti-DHC	ThermoFisher Scientific	PA5-49373; RRID:AB_2634827
sheep anti-Bub1	Gift from S. Taylor	N/A
rabbit anti-Septin-2	Novus Biologicals	NBP1-85212; RRID:AB_11002313
mouse anti-Ska3	Santa Cruz Biotechnology	sc-390326; RRID:AB_2923182
rabbit anti-CEP90	Novus Biologicals	NBP2-56805; RRID:AB_2923183
mouse anti-Ska2	Santa Cruz Biotechnology	sc-514495; RRID:AB_2923184
mouse anti-4.1r (B-11)	Santa Cruz Biotechnology	sc-166759; RRID:AB_2098363
rabbit anti-Astrin (N-terminal)	Gift from D. Compton	N/A
rabbit anti-Kif4a	ThermoFisher Scientific	pa5-30492; RRID:AB_2547966
rat anti-CLASP1	Maffini et al.[73]	N/A
rat anti-CLASP2	Maffini et al.[73]	N/A
rabbit anti-BubR1	Abcam	Ab4637; RRID:AB_2066074
mouse anti-Nde1	Abnova	H00054820-M01; RRID:AB_425994
rabbit anti-SHP2	Abcam	Ab10555; RRID:AB_297290
rabbit anti-survivin	Novus Biologicals	NB500-201; RRID:AB_10001517
mouse anti-GAPDH	Proteintech	60004-1-Ig; RRID:AB_2107436
rabbit anti-vinculin	ThermoFisher Scientific	700062; RRID:AB_2532280
rabbit anti-Mis12	Gift from C. Sunkel	N/A
rabbit anti-Kif18a	Bethyl Laboratories	A301-079A; RRID:AB_873056
rabbit anti-KNL1	Novus Biologicals	NBP2-92855; RRID:AB_2923185
rabbit anti-Nsl1	Novus Biologicals	NBP2-58614; RRID:AB_2923186
rabbit anti-Ska1	Gift from P. Meraldi	N/A
goat anti-TACC3	Novus Biologicals	AF5720-SP; RRID:AB_2923187
rabbit anti-Zw10	Novus Biologicals	NBP2-38644; RRID:AB_2923188
rabbit anti-CENP-E	Abcam	Ab133583; RRID:AB_2910100
rabbit anti-CENP-I	Gift from P. Meraldi	N/A
rabbit anti-CENP-H	Novus Biologicals	NBP1-82546; RRID:AB_11032306
rabbit anti-CENP-N	Novus Biologicals	NBP1-79664; RRID:AB_11004955

(*Continued on next page*)

Continued		
REAGENT or RESOURCE	SOURCE	IDENTIFIER
rabbit anti-LRRCC1/CLERC	Abcam	Ab95450; RRID:AB_10680341
Goat anti-mouse Alexa Fluor 488	Thermo Fisher Scientific	Cat# A-11029; RRID:AB_2534088
Goat anti-mouse Alexa Fluor 568	Thermo Fisher Scientific	Cat# A-11031; RRID:AB_144696
Goat anti-rabbit Alexa Fluor 568	Thermo Fisher Scientific	Cat# A-11011; RRID:AB_143157
Goat anti- guinea pig Alexa Fluor 568	Thermo Fisher Scientific	Cat# A-21450; RRID:AB_2735091
anti-mouse-HRP	Jackson ImmunoResearch Laboratories	Cat#115-035-003; RRID:AB_10015289
anti-rabbit-HRP	Jackson ImmunoResearch Laboratories	Cat#111-035-003; RRID:AB_2313567
anti-sheep-HRP	Jackson ImmunoResearch Laboratories	Cat#713-035-003; RRID:AB_2340709
anti-rat-HRP	Jackson ImmunoResearch Laboratories	Code: 112-035-143; RRID:AB_2338138
anti-goat-HRP	Jackson ImmunoResearch Laboratories	Cat#305-035-003; RRID:AB_2339400
Chemicals, peptides, and recombinant proteins		
Nocodazole	Sigma-Aldrich	Cat#M1401
MG132	EMD Millipore	Cat#133407-82-6
Monastrol	Tocris	Cat#1305
Deposited data		
Additional videos and quantifications for all analyzed siRNAs	This paper	http://chromosomecongression.i3s.up.pt
Experimental models: Cell lines		
Human HeLa parental	Gift from Y.Mimori-Kiyosue	N/A
Human HeLa H2B-GFP, α-tubulin-mRFP	Generated by lentiviral transduction	N/A
Human HeLa Mad2-GFP	Schweizer et al.[74]	N/A
Human HeLa Cyclin B1-Venus	Gift from J. Pines	N/A
Human HeLa Cyclin B1-Venus, H2B-mRFP	Generated by lentiviral transduction	N/A
Human U2OS parental	Gift from S. Geley	N/A
Human U2OS H2B-GFP, mCherry-α-tubulin	Gift from S. Geley	N/A
Human hTERT-RPE-1 (RPE-1) parental	Gift from Ben Black	N/A
Human RPE-1 H2B-GFP, mCherry-α-tubulin	Generated by lentiviral transduction	N/A
Human RPE-1 Cyclin B1-Venus	Gift from J. Pines	N/A
Human RPE-1 Cyclin B1-Venus, H2B-mRFP	Generated by lentiviral transduction	N/A
Oligonucleotides		
Data S2	N/A	N/A
Software and algorithms		
Fiji/ImageJ	ImageJ	N/A
Nikon Elements	Nikon Instruments	https://www.microscope.healthcare.nikon.com/products/software/nis-elements

RESOURCE AVAILABILITY

Lead contact

Further information and requests for resources and reagents should be directed to and will be fulfilled by the lead contact, Helder Maiato (maiato@i3s.up.pt).

Materials availability

All reagents generated in this study are available from the lead contact without restriction.

Data and code availability

- A public repository where time-lapse videos, phenotypical fingerprints, siRNA sequences and available western blotting analysis for each condition can be conveniently browsed and is freely available as a community resource at http://chromosomecongression.i3s.up.pt.
- This paper does not report original code.
- Any additional information required to reanalyze the data reported in this paper is available from the lead contact upon request.

EXPERIMENTAL MODEL AND SUBJECT DETAILS

Cell lines

All cell lines were cultured at 37°C in 5% CO_2 atmosphere in Dulbecco's modified medium (DMEM, Gibco, Thermofisher) containing 10% fetal bovine serum (FBS, Gibco, Thermofisher). HeLa H2B-GFP/α-tubulin-mRFP, HeLa Cyclin B1-Venus/H2B-mRFP, RPE-1 H2B-GFP/mCherry-α-tubulin and RPE-1 Cyclin B1-Venus/H2B-mRFP cells were generated by lentiviral transduction. HeLa parental was kindly provided by Y. Mimori-Kiyosue (RIKEN, Japan). U2OS parental and H2B-GFP/mCherry-α-tubulin were kindly provided by S. Geley (Innsbruck Medical University, Innsbruck, Austria). hTERT-RPE-1 (RPE-1) parental (ATCC CRL-400) was kindly provided by Ben Black (U. Pennsylvania, PA, USA). HeLa Mad2-GFP cells were previously described.[74] HeLa and RPE-1 cells expressing Cyclin B1-Venus were kindly provided by J. Pines (Cancer Research Institute, London, UK).

METHOD DETAILS

High-content live-cell imaging RNAi screen

All siRNA sequences used were either a commercial predesigned siRNA from Sigma-Aldrich (MISSION siRNA) or Dharmacon, many of which were previously validated by other published studies (see Data S2). For each protein, depletion efficiency was first optimized after preliminary phenotypic analysis between 24-96 h upon siRNA transfection (for specific conditions see Data S1) and confirmed by western blotting whenever antibodies against specific proteins were available (Data S3). For few proteins whose role in chromosome congression remained unclear at the mechanistic level or were followed-up in subsequent experiments, a second siRNA was used to rule-out possible off-targeting effects. This led to the identification of six proteins (Shp2, GAK, CEP72, CEP90, CENP-H and Mis12), where no discernable congression phenotype was observed with the second siRNA, despite a clear reduction in protein levels with both siRNA sequences (Figure S1), or a clear congression phenotype was observed despite no evident reduction in protein levels with two siRNA sequences, suggesting that they are off-targets. A second siRNA was also used to validate all selected conditions that were followed-up to determine the origin of micronuclei (Data S2). Whenever the results obtained with the second siRNA oligonucleotide were consistent with those obtained with the original siRNA oligonucleotide, the data from both experiments was pooled for statistical analysis. All exceptions (Arp1, Haspin, CENP-F, HAUS4 and CENP-T) that could not be validated by western blotting due to the poor quality of the antibodies we had access to are clearly marked in the respective figures and main text, and were not followed-up in subsequent experiments. Treatment with scramble siRNA was undistinguishable from mock transfection (Lipofectamine only) and was therefore used as a negative control throughout the manuscript. A total of 125 proteins were analyzed in this study (Data S1). For high-content live-cell imaging, HeLa cells stably expressing H2B-GFP/α-tubulin-mRFP were plated onto 96-well plate in DMEM supplemented with 5% FBS and after 1 h transfected with siRNA oligonucleotides (Data S2) at a final concentration of 50 nM. Transfections were performed using Lipofectamine RNAiMAX in Opti-MEM medium (both from Thermo Fisher Scientific) according to the manufacturer's instructions. Transfection medium was replaced with complete medium after 6 h. For time-lapse microscopy acquisition, cell culture medium was changed to DMEM without phenol red supplemented with 10% FBS 6-12 h before acquisition. Cells were imaged for 72 h in an IN CELL Analyzer 2000 microscope (GE Healthcare, Chicago, IL, USA) equipped with temperature and CO_2 controller, using a Nikon 20x/0.45 NA Plan Fluor objective according to manufacturer instructions. For some validation experiments with a second siRNA oligonucleotide a Nikon ECLIPSE TI microscope (Nikon, Japan) equipped with temperature and CO_2 controller, using a Nikon 20x/0.45 NA Plan Fluor objective according to the manufacturer's instructions, using 24-well plates. Single planes were acquired every 10 min for approximately 72 h. Images were processed using ImageJ software. Long-term recordings of HeLa Cyclin B1-venus treated with nocodazole and MG132 were also performed under similar conditions using the same IN CELL Analyzer 2000 microscope system, imaged every 15 min for 13 h.

Other RNAi experiments

For high-resolution live cell imaging and immunofluorescence analysis of CENP-E depletion (siCENP-E), cells were plated at 50-60% confluence onto 22 x 22 mm No. 1.5 glass coverslips in DMEM supplemented with 5% of FBS. RNAi transfection was performed using Lipofectamine RNAiMAX reagent (Thermofisher) with 20 nM of siRNA against human CENP-E (see siRNA sequence in Data S2), diluted in serum-free media (Opti-MEM, Thermofisher). Depletion of CENP-E was maximal at 24 h after siRNA transfection and all of the analysis was performed at 24 h.

Drug treatments

Microtubule depolymerization was induced by nocodazole (Sigma-Aldrich) at 1 μM. To inhibit the proteasome, induce a metaphase arrest, and prevent exit due to a compromised SAC, cells were treated with 5 μM MG132 (EMD Millipore). To promote chromosome missegregation, a monastrol washout assay was performed. Briefly, cells were incubated during 8-10 h with 100 μM monastrol. After this period, monastrol was washed twice with warm PBS followed by washing with warm fresh medium and entry in anaphase was monitored under the microscope.

High-resolution time-lapse microscopy

For high-resolution time-lapse microscopy, cells were plated onto 22 x 22 mm No. 1.5 glass coverslips (Corning) and cell culture medium was changed to phenol-red-free DMEM CO_2-independent medium (Invitrogen) supplemented with 10% FBS 6-12 h before mounting. Coverslips were mounted onto 35-mm magnetic chambers (14 mm, no. 1.5, MaTek corporation) immediately before imaging. Time-lapse imaging was performed in a heated chamber (37°C) using a 100x oil-immersion 1.40 NA Plan-Apochromatic objective mounted on an inverted microscope (Eclipse TE2000U; Nikon) equipped with a CSU-X1 spinning-disk confocal head (Yokogawa Corporation of America) controlled by NIS-Elements software and with three laser lines (488nm, 561nm, and 647 nm). Images were detected with a iXonEM+ EM-CCD camera (Andor Technology). Images of U2OS and RPE-1 expressing H2B-GFP, mCherry-α-tubulin were collected every 2 minutes or 30 seconds: 9 x 2 μm z-stacks spanning a total volume of 16 μm. For imaging of HeLa Mad2-GFP and HeLa and RPE-1 expressing Cyclin-B1-Venus/H2B-mRFP eleven 1-μm-separated z-planes covering the entire volume of the mitotic spindle were collected every 2 min. All displayed images represent maximum-intensity projections of Z-stacks, analysed with the open source image analysis software ImageJ.

Immunofluorescence microscopy

For immunofluorescence processing, cells were fixed with 4% Paraformaldehyde (Electron Microscopy Sciences) for 10 min followed by extraction with 0.3% Triton X-100 in PBS (Sigma-Aldrich) for 10 min. After blocking with 10% FBS in PBS with 0.1% Triton X-100, all primary antibodies were incubated at 4°C overnight. Then, the cells were washed with PBS containing 0.1% Triton X-100 and incubated with the respective secondary antibodies for 1 h at room temperature. Primary antibodies used were: mouse anti-Mad1 (1:500; Merck Millipore); mouse anti α-tubulin (1:2000; Sigma); rabbit anti-β-tubulin (1:2000; Abcam); anti-guinea pig CENP-C (1:1000; MBL International). Secondary antibodies used were Alexa Fluor 488, Alexa Fluor 568 and Alexa Fluor 647 (1:1000; Themofisher). DNA was counterstained with 1 μg/mL DAPI (4',6'-diamino-2-fenil-indol; Sigma-Aldrich) and mounted onto glass slides with 20 mM Tris pH8, 0.5 N-propyl gallate and 90% glycerol. Images were acquired using an AxioImager Z1 (63x, Plan oil differential interference contract objective lens, 1.46 NA; from Carl Zeiss), coupled with a CCD camera (ORCA-R2; Hamamatsu Photonics) and the Zen software (Carl Zeiss). Blind deconvolution of 3D image datasets was performed using Autoquant X software (Media Cybernetics).

Western Blotting

Cell extracts were collected after trypsinization and centrifuged at 1200 rpm for 5 min, washed and re-suspended in Lysis Buffer (NP-40, 20 nM HEPES/KOH pH 7.9; 1 mM EDTA pH 8; 1 mM EGTA; 150 mM NaCl; 0.5% NP40; 10% glycerol, 1:50 protease inhibitor; 1:100 Phenylmethylsulfonyl fluoride). The samples were then flash frozen in liquid nitrogen and kept on ice for 30 min. After centrifugation at 14000 rpm for 20 min at 4°C the supernatant was collected and protein concentration determined by the Bradford protein assay (Bio-Rad). Fifty micrograms of total extract were then loaded in SDS-polyacrylamide gels and transferred onto nitrocellulose membranes for western blot analysis. The membranes were blocked with 5% milk in TBS with 0.1% Tween-20 (TBS-T) at room temperature during 1 h, and all primary antibodies were incubated at 4°C overnight. After three washes in TBS-T the membranes were incubated with the secondary antibody for 1 h at room temperature. The membranes were washed in the same conditions than previously and the detection was performed with Clarity Western ECL Substrate (Bio-Rad). The following antibodies were used for western blot: mouse anti-Hec1 (9GA) (1:500; Abcam), mouse anti-Dsn1 (1:1000; a gift from Andrea Musacchio, MPI, Dortmund, Germany), rabbit anti-CENP-E (1:250; Abcam), mouse anti-Aim1 (1:1000; BD Bioscience), mouse anti-ATRX (1:1000; Santa Cruz Biotechnology), rabbit anti-CEP72 (1:1000; Novus Biologicals), mouse anti-GAK (1:500; R&D Systems), rabbit anti- WDHD1/And-1 (1:1000; Novus Biologicals), rabbit anti-Aurora-A (1:1000; Novus Biologicals), rabbit anti-HURP (1:500, a gift from Patrick Meraldi), mouse anti-INCENP (1:500; Santa Cruz Biotechnology), rabbit anti-LRRCC1/CLERC (1:1000; Abcam), mouse anti-Sgo-1 (F-8) (1:1000; Santa Cruz Biotechnology), rabbit anti-DHC (1:500; ThermoFisher Scientific), mouse anti-Nde1 (1:1000; Abnova), sheep anti-Bub1 (1:1000; a gift from Stephen Taylor); rabbit anti-Septin-2 (1:500; Novus Biologicals), rabbit anti-CEP90/PIBF1 (1:1000; Novus Biologicals), mouse anti-Ska2 (1:1000; Santa Cruz Biotechnology), mouse anti-4.1r (B-11) (1:1000; Santa Cruz Biotechnology), rabbit anti-Astrin (N-terminal) (1:500; a gift from Duane Compton), rabbit anti-Kif4a (1:1000; ThermoFisher Scientific), rat anti-CLASP1 (1:50; Maffini et al., 2009), rat anti-CLASP2 (1:50; Maffini et al., 2009), rabbit anti-BubR1 (1:1000; Abcam), rabbit anti-SHP2 (1:1000; Abcam), rabbit anti-survivin (1:1000; Novus Biologicals), mouse anti-Ska3 (1:500; Santa Cruz Biotechnology), rabbit anti-Mis12 (1:1000, a gift from Claudio Sunkel), rabbit anti-Kif18a (1:1000; Bethyl Laboratories), rabbit anti-KNL1 (1:1000; Novus Biologicals), rabbit anti-Nsl1 (1:500, Novus Biologicals), rabbit anti-Ska1 (1:500; a gift from Patrick Meraldi), goat anti-TACC3 (1:1000; Novus Biologicals), rabbit anti-Zw10 (1:1500; Novus Biologicals), rabbit anti-CENP-I (1:250; a gift from Patrick Meraldi), rabbit anti-CENP-H (1:500; Novus Biologicals), rabbit anti-CENP-N (1:500; Novus Biologicals), rabbit anti-CLERC (1:500, Abcam), mouse anti-GAPDH (1:40000; Proteintech), rabbit anti-vinculin (1:1000;ThermoFisher Sientific), mouse anti-α-tubulin (clone B-512; 1:5000;

Sigma-Aldrich) were used as primary antibodies, and anti-mouse-HRP, anti-rabbit-HRP, anti-sheep-HRP, anti-rat-HRP and anti-goat-HRP were used as secondary antibodies (1:5000; Jackson ImmunoResearch Laboratories,).

QUANTIFICATION AND STATISTICAL ANALYSIS

Quantification of mitotic errors

Mitotic errors were tracked and quantified manually through the assessment of H2B localization in single plane images. Mitotic errors were divided into 3 main classes: lagging chromosomes, DNA bridges or misaligned chromosomes and these were discriminated according to location and morphology associated with H2B localization. Lagging chromosomes retained normal DNA condensation and emerged at different stages during anaphase. Any H2B-positive material between the two chromosomes masses, but distinguishably separated from them, was counted as lagging chromosomes. DNA bridges were characterized by stretches of DNA that connected both daughter nuclei and often displayed aberrant DNA condensation as judged by H2B localization. Misaligned chromosomes were characterized by any H2B-positive material that remained near the spindle pole or clearly outside the metaphase plate. To determine micronuclei origin, fully formed micronuclei were backtracked to reveal whether these originated from lagging chromosomes, DNA bridges or misaligned chromosomes. The absolute probability of micronucleus formation from a lagging chromosome was determined by the ratio between the number of daughter cells with micronuclei derived from lagging chromosomes and the total number of cells with lagging chromosomes. The absolute probability of micronucleus formation from a DNA bridge was determined by the ratio between the number of daughter cells with micronuclei derived from DNA bridges and the total number of cells with DNA bridges. The absolute probability of micronucleus formation from a misaligned chromosome was determined by the ratio between the number of daughter cells with micronuclei derived from misaligned chromosomes and the total number of cells that exit mitosis with a misaligned chromosome. For the relative probabilities, the sum of the 3 independent absolute probability values was normalized to 1.

Quantitative image analysis

For quantification of Mad1 fluorescence intensity, images were analysed using ImageJ. Briefly, individual kinetochores were identified by CENP-C staining and marked by a region of interest (ROI). The average fluorescence intensity of signals of Mad1 at kinetochores was measured on the focused z plan. The background signal was measured within a neighbouring region and was subtracted from the measured fluorescence intensity the region of interest. Fluorescence intensity measurements were normalized to the CENP-C signals. Mad1 negative values were considered zero, since resulted from the high background fluorescence observed in early anaphase cells. Approximately 90 kinetochore pairs from 9 cells were analysed for control prometaphase cells, 72 kinetochore pairs from 14 cells for prometaphase in CENP-E depleted cells and 19 kinetochore pairs from 14 cells for early anaphase in CENP-E depleted cells. The fluorescence levels of Cyclin B1 in HeLa cells treated with nocodazole were measured using the IN Cell Developer Toolbox software (GE Healthcare). After background subtraction, fluorescence intensities were normalized to the level at time = 0 and represented as a function of time. The levels of Cyclin B1 in siScramble, siCENP-E, siTACC3 HeLa cells and siScramble, siCENP-E RPE-1 were measured using ImageJ. A small square region of interest (ROI) was defined, and Cyclin B1 fluorescence intensity measured, throughout time in the cell. The same ROI was used to measure the background outside the region of interest. All fluorescence intensity values were then background corrected and the values were normalized at 14 or 8 minutes before anaphase onset in HeLa and RPE-1 cells, respectively. The microtubule depolymerization rate after nocodazole treatment in U2OS and RPE-1 cells was determined by the proportion of total and soluble α-tubulin levels. The total α-tubulin intensity was measured by drawing a larger oval shaped region of interest (ROI) contained the entire cell in sum-projected images (ImageJ). The soluble α-tubulin levels were determined by drawing five smaller oval shaped ROI outside the chromosome region and the average of these values were calculated in sum-projected images. The fluorescence intensities were normalized to the level at time = 0 and represented as a function of time.

Statistical analysis

All results presented in this manuscript were obtained from pooling data from at least 2 independent experiments unless otherwise stated. Sample sizes and statistical tests used for each experiment are indicated in the respective figure legends. Quantifications of mitotic errors (i.e. cell death and micronuclei) were analyzed using the Fisher's exact two-tailed test. Correlations were calculated using two-tailed Pearson's correlation coefficients. When only two experimental groups were compared, we used either a parametric t test or a nonparametric Mann-Whitney test. Distribution normalities were assessed using the D'Agostino-Pearson omnibus test. For the comparison of the single exponential fitting curve extra sum-of square F test was used. Probabilities were calculated using Chi-squared test. For each graph, where applicable, ns= non-significant, *$p \leq 0.05$, **$p \leq 0.01$ ***$p \leq 0.001$ and ****$p \leq 0.0001$, unless stated otherwise. In all plots error bars represent standard deviation. All statistical analysis was performed using GraphPad Prism V7 (GraphPad Software).

Current Biology, Volume *32*

Supplemental Information

Micronuclei from misaligned chromosomes that satisfy the spindle assembly checkpoint in cancer cells

Ana Margarida Gomes, Bernardo Orr, Marco Novais-Cruz, Filipe De Sousa, Joana Macário-Monteiro, Carolina Lemos, Cristina Ferrás, and Helder Maiato

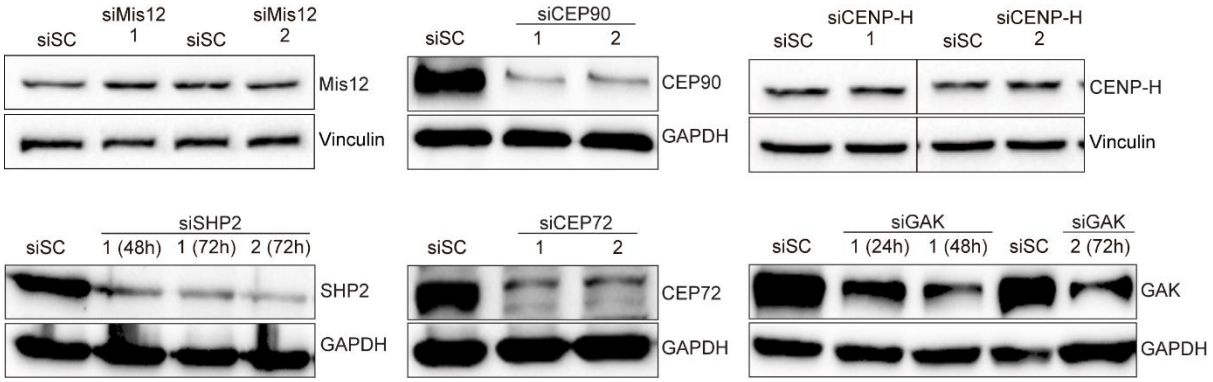

Figure S1. Identification of off-targets, related to Figure 1. Protein lysates obtained after RNAi treatment were immunoblotted with an antibody specific for each protein of interest (Mis12, CEP90, CENP-H, SHP2, CEP72 and GAK, upper bands). The bottom band corresponds to antibody detection of GAPDH or Vinculin, which were used as loading controls.

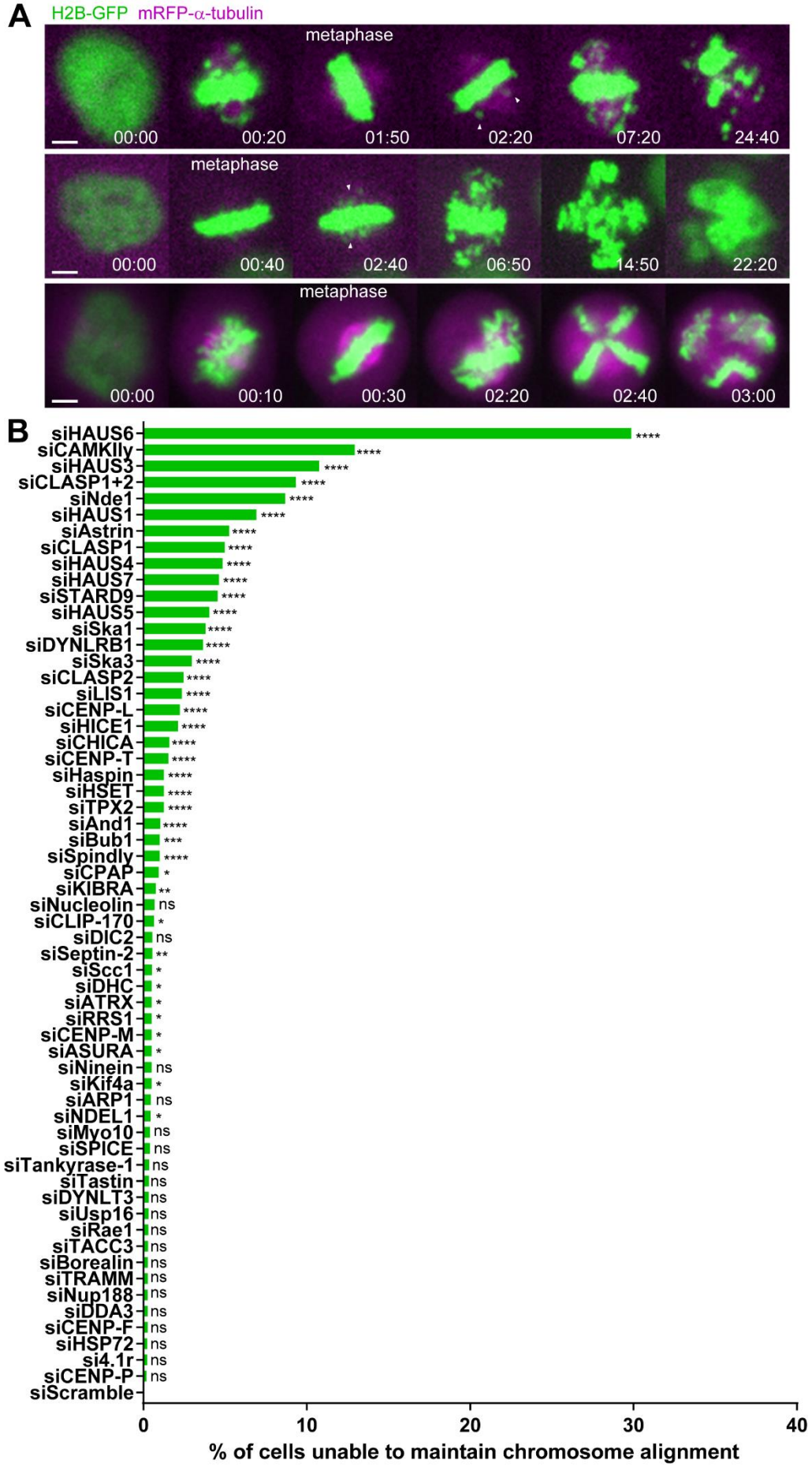
A
H2B-GFP mRFP-α-tubulin
metaphase
00:00
00:20
01:50
02:20
07:20
24:40
metaphase
00:00
00:40
02:40
06:50
14:50
22:20
metaphase
00:00
00:10
00:30
02:20
02:40
03:00
B
siHAUS6 ****
siCAMKIIγ ****
siHAUS3 ****
siCLASP1+2 ****
siNde1 ****
siHAUS1 ****
siAstrin ****
siCLASP1 ****
siHAUS4 ****
siHAUS7 ****
siSTARD9 ****
siHAUS5 ****
siSka1 ****
siDYNLRB1 ****
siSka3 ****
siCLASP2 ****
siLIS1 ****
siCENP-L ****
siHICE1 ****
siCHICA ****
siCENP-T ****
siHaspin ****
siHSET ****
siTPX2 ****
siAnd1 ****
siBub1 ***
siSpindly ****
siCPAP *
siKIBRA **
siNucleolin ns
siCLIP-170 *
siDIC2 ns
siSeptin-2 **
siScc1 *
siDHC *
siATRX *
siRRS1 *
siCENP-M *
siASURA *
siNinein ns
siKif4a *
siARP1 ns
siNDEL1 *
siMyo10 ns
siSPICE ns
siTankyrase-1 ns
siTastin ns
siDYNLT3 ns
siUsp16 ns
siRae1 ns
siTACC3 ns
siBorealin ns
siTRAMM ns
siNup188 ns
siDDA3 ns
siCENP-F ns
siHSP72 ns
si4.1r ns
siCENP-P ns
siScramble
0
10
20
30
40
% of cells unable to maintain chromosome alignment

Figure S2. In addition to chromosome alignment defects, some genetic conditions also compromise the maintenance of chromosome alignment at the metaphase plate, related to Figure 2. a) Examples of time-lapse sequences illustrating the three main mitotic phenotypes of chromosome alignment maintenance defects observed: 1) cells showed a prolonged delay in chromosome alignment but eventually completed congression, after which chromosomes/chromatids underwent gradual scattering from the metaphase plate; 2) chromosomes aligned normally at the metaphase plate, but then underwent gradual scattering; 3) chromosomes aligned normally at the metaphase plate, followed by spindle pole fragmentation and chromosome scattering. Arrows indicate scattered chromosomes/chromatids in cells that were unable to maintain chromosome alignment at the metaphase plate. Scale bar = 5 µm. Time: h:min, from nuclear envelope breakdown (NEB) to cell death or mitotic exit. **b)** Frequency of cells exhibiting problems in the maintenance of chromosome alignment at the metaphase plate. Only the conditions exhibiting problems in the maintenance of chromosome alignment were included. At least 2 independent experiments were analyzed. The total number of cells analyzed for each condition is indicated in Table S1. (*p≤0.05, **p≤0.01, ***p≤0.001, ****p≤0.0001, ns corresponds to not significantly different from control, Fisher´s exact two-tailed test).

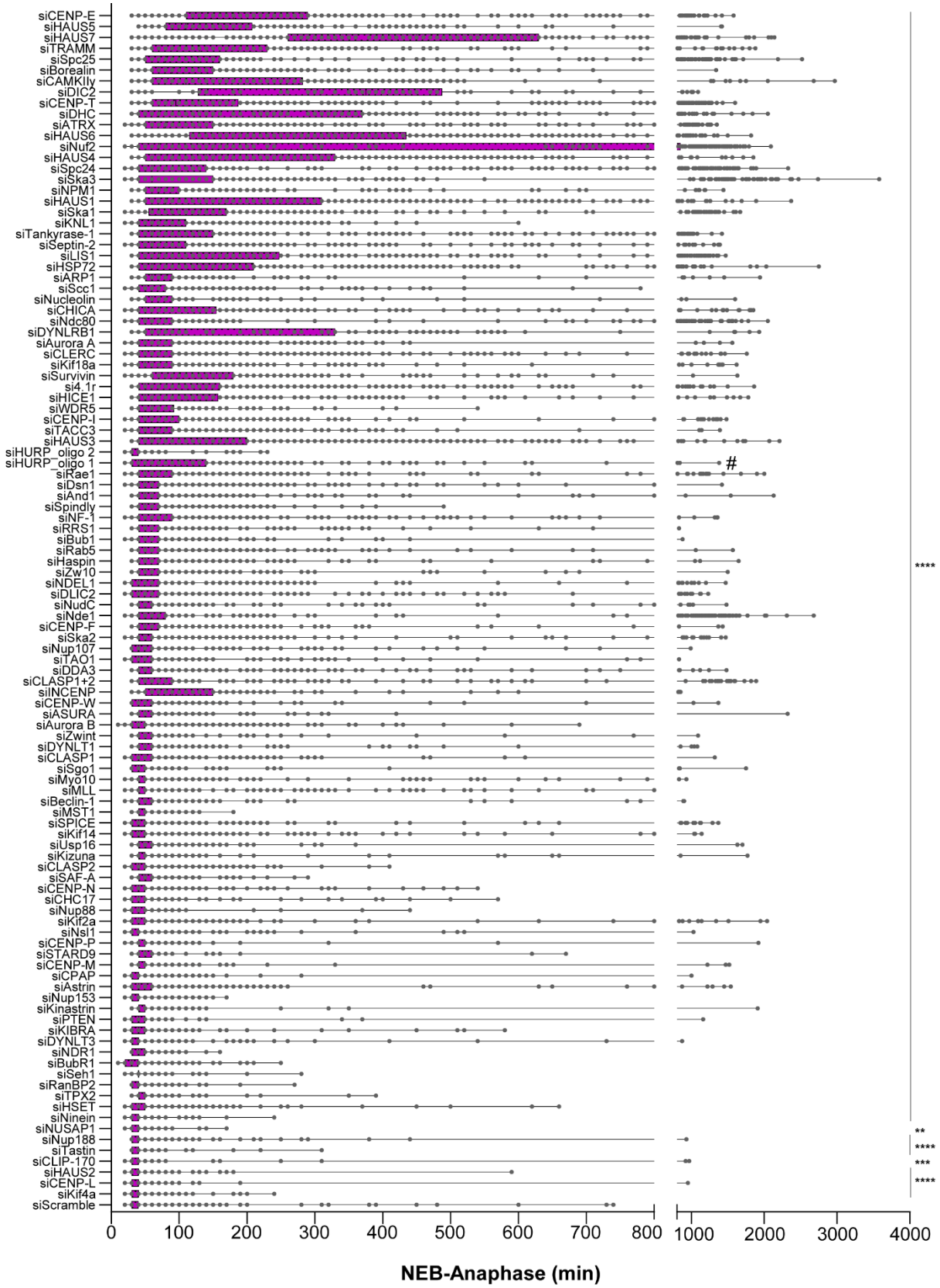

Figure S3. Mitotic duration upon gene-specific RNAi-mediated depletion, related to Figure 3. HeLa cells stably expressing H2B-GFP and α-tubulin-mRFP were

acquired every 10 minutes. Mitotic duration was determined by measuring the time between nuclear envelope breakdown (NEB) and anaphase onset, shown in minutes. Data was presented as box-and-whiskers and each point corresponds to one cell. The difference between mean values of each RNAi condition was statistically significant from the control mean values. At least 2 independent experiments per condition were performed. (*p≤0.05, **p≤0.01, ***p≤0.001, ****p≤0.0001, ns corresponds to not significantly different from control, Mann-Whitney test).

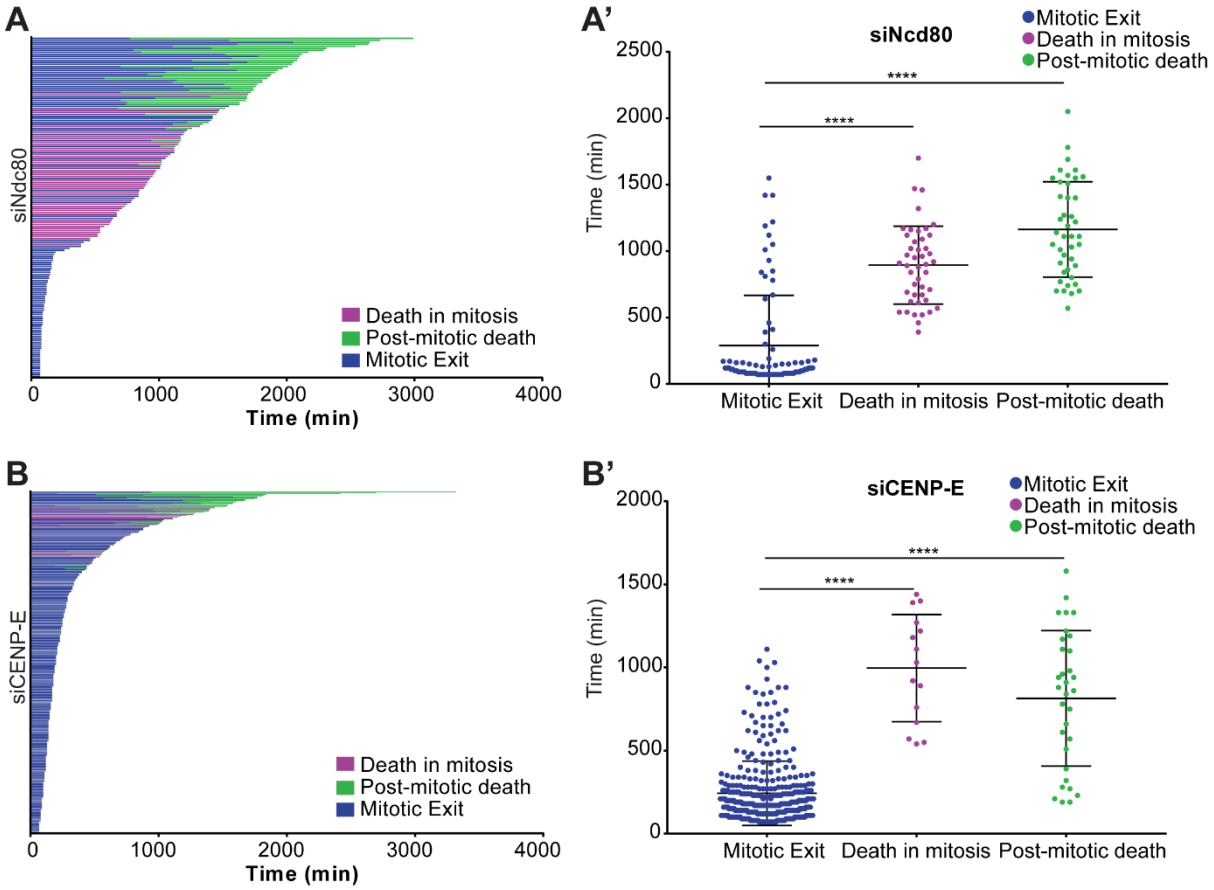

Figure S4. Cell fate upon induction of chromosome alignment defects of distinct molecular nature, related to Figure 3. a) Cell fate profiles of HeLa cells with delayed or failed chromosome alignment after Ndc80 depletion. Each line indicates a single cell and respective outcome. **a´)** Time that cells spent until mitotic exit (blue), death in mitosis (purple) or in subsequent interphase (green) after Ndc80 depletion. Each dot represents a single cell. The horizontal line indicates the mean of all quantified cells and the error bars represent the standard deviation from a pool of four independent experiments (Mitotic exit, 289±377 min, n=83; Death in mitosis, 894±292 min, n=45; Post-mitotic death 1162±359 min, n=42; ****p≤0.0001 relative to control, analyzed using a Mann-Whitney Test). **b)** Cell fate profiles of HeLa cells with delayed or failed chromosome alignment after CENP-E depletion. **b´)** Time that cells spent until mitotic exit (blue), death in mitosis (purple) or in the subsequent interphase (green) after

CENP-E depletion. Each dot represents a single cell. The horizontal line indicates the mean of all quantified cells and the error bars represent the standard deviation from a pool of five independent experiments (Mitotic exit, 243±193 min, n=358; Death in mitosis 996±322 min, n=15; Post-mitotic death 814±408 min, n=32; ****p≤0.0001 relative to control, analyzed using a Mann-Whitney Test).

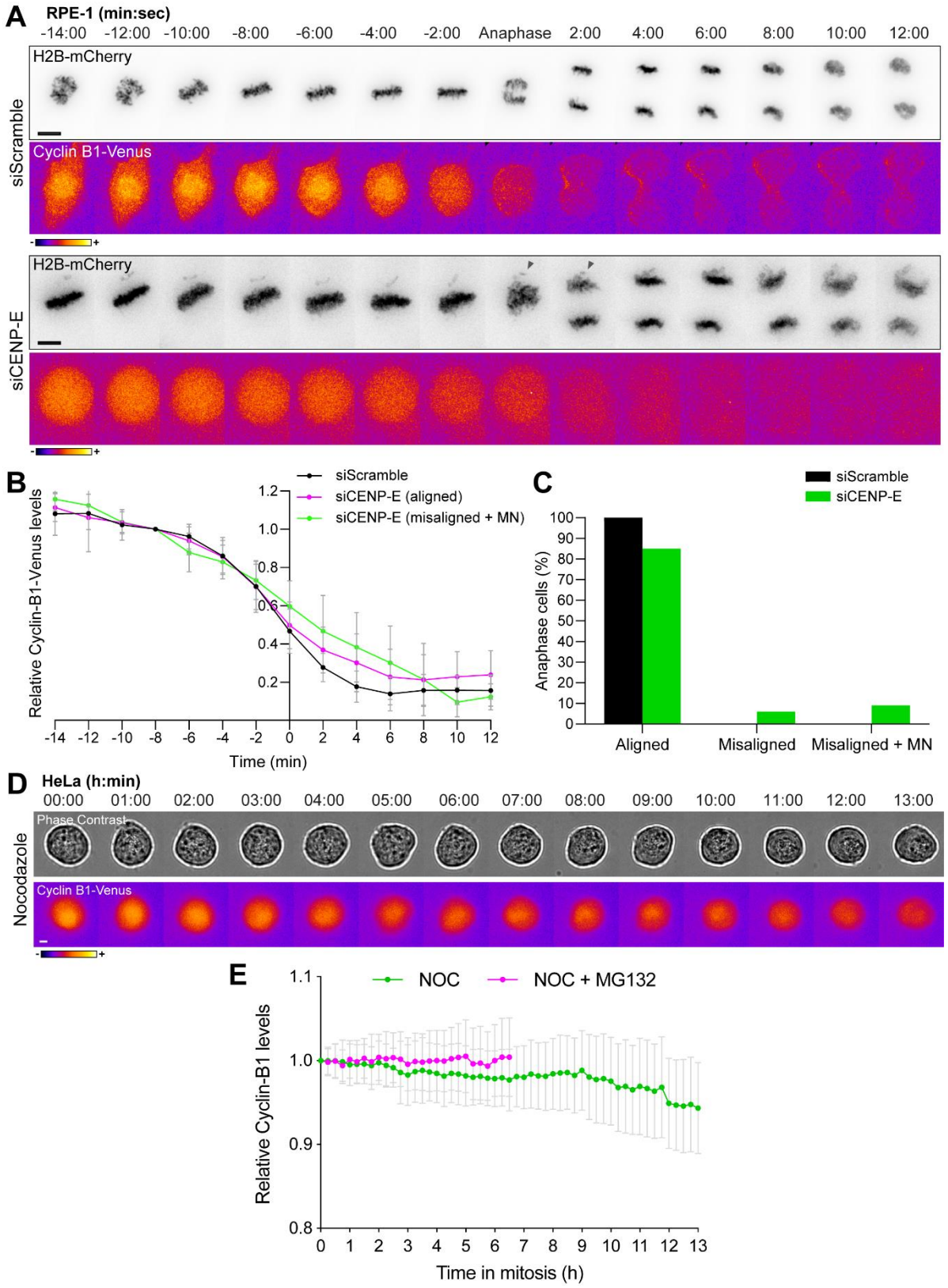

Figure S5. Further characterization of Cyclin B1 degradation profiles in RPE-1 and HeLa cells, related to Figure 5. a) Selective time frames from live-cell

microscopy of RPE-1 cells stably expressing H2B-mRFP and Cyclin B1-Venus in control and siCENP-E. Images were acquired every 2 min. Time = min:sec. Time 00:00 = anaphase onset. Black arrowheads point to misaligned chromosomes that remain upon anaphase onset. **b)** Cyclin B1 degradation profile for control, CENP-E- depleted cells that properly align their chromosomes at the metaphase plate and CENP-E-depleted cells that exit mitosis with misaligned chromosomes give rise to micronuclei. Fluorescence intensities were normalized to the levels at time = -8. The curves represent mean Cyclin B1-Venus fluorescence intensity from all analyzed cells and errors bars represent the standard derivation from a pool of three independent experiments (siScramble n=30; siCENP-E (aligned) n=30; siCENP-E (misaligned+micronuclei) n=5). **c)** Frequency of anaphase cells with aligned chromosomes, misaligned chromosomes and misaligned chromosomes that result in micronuclei in control (black bars) and CENP-E-depleted cells (green bars). **d)** Selected time frames from phase-contrast and fluorescence microscopy of Cyclin B1-Venus HeLa cells treated with nocodazole with or without MG132. Images were acquired every 15 min. Scale bar = 5 µm. Time = h:min. **e)** Cyclin B1 degradation profiles of nocodazole-treated Cyclin B1-Venus HeLa cells in the presence or absence of MG132. Fluorescence intensities were normalized to the levels at time = 0. The curves depict mean Cyclin B1-Venus fluorescence intensity from all analyzed cells per condition (nocodazole n=12; nocodazole + MG132 n=10), and error bars represent the standard deviation. Note that acquisition in the presence of MG132 was terminated earlier relative to acquisition without MG132 due to cell death.

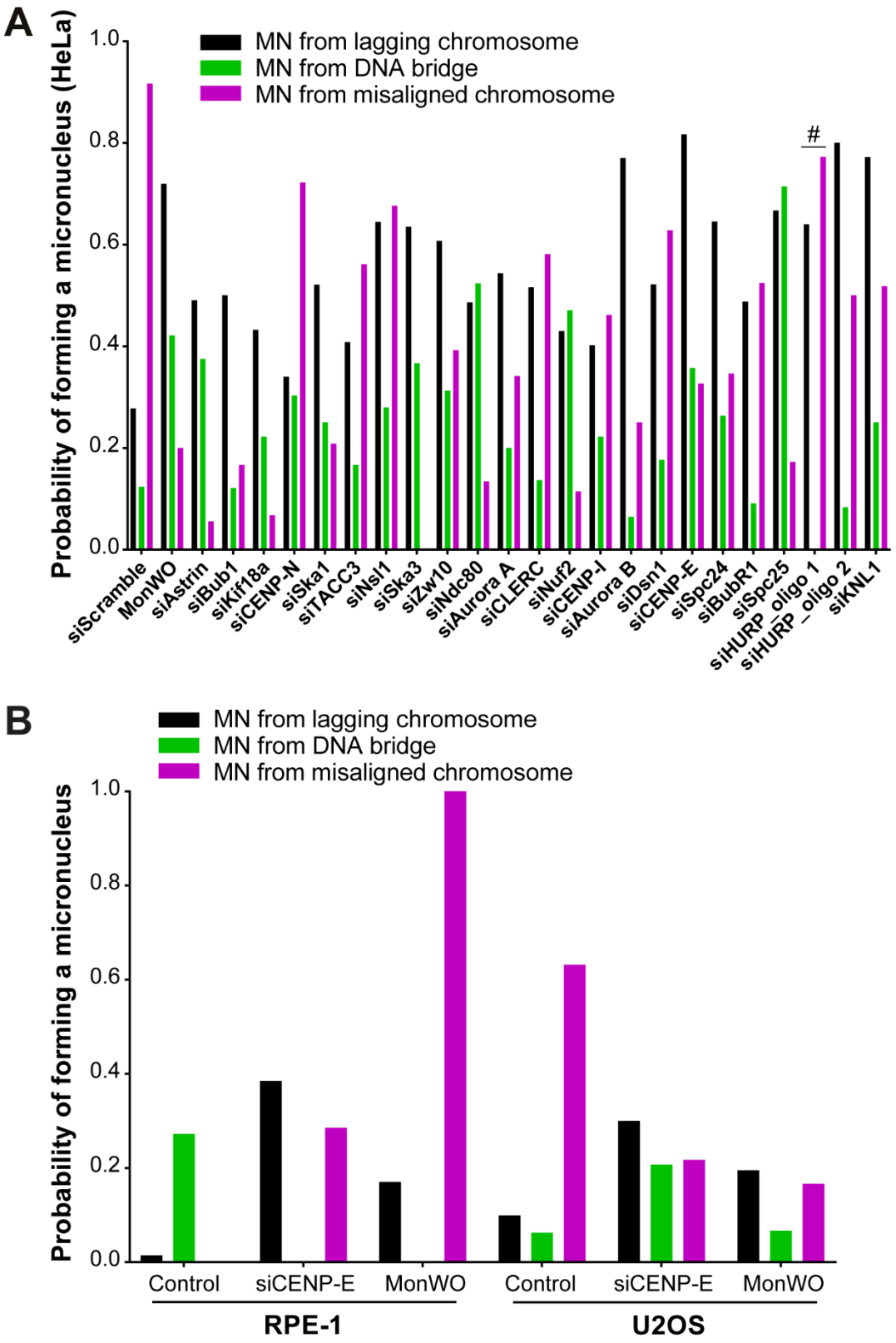

Figure S6. Absolute probabilities of forming a micronucleus from misaligned chromosomes, DNA bridges and lagging chromosomes in the different cell lines used, related to Figure 6 and Figure 7. a) Absolute probabilities of forming a

micronucleus of different origins in unperturbed HeLa cells and after molecular perturbations that weaken kinetochore-microtubule attachments or promote the formation of anaphase lagging chromosomes after monastrol treatment and washout (MonWO). [siScramble n=1700, MonWO n=327, siAstrin n=423, siBub1 n=457, siKif18a n= 540, siCENP-N n= 422, siSka1 n=395, siTACC3 n=485, siNsl1 n=400, siSka3 n= 383, siZw10 n= 404, siNdc80 n=440, siAurora A n= 388, siCLERC n=263, siNuf2 n=428, siCENP-I n= 389, siAurora B n=499, siDsn1 n=688, siCENP-E n= 346, siSpc24 n=418, siBubR1 n=387, siSpc25 n= 425, siHURP_oligo1 n=296, siHURP_oligo2 n=200, siKNL1 n=413; pool of 2 independent experiments for each siRNAi oligonucleotide per condition, with the exception of Aurora A and CLERC in which only 1 experiment for the second siRNAi oligonucleotide was performed. All independent experiments were pooled]. **b)** Absolute probabilities of forming a micronucleus of different origins in unperturbed RPE-1 and U2OS cells and after CENP-E depletion (siCENP-E) or monastrol treatment and washout. [RPE-1 cells: control, n=163; siCENP-E, n=95; MonWO, n=105]. [U2OS cells: control, n=250; siCENP-E, n=81; MonWO, n=49].

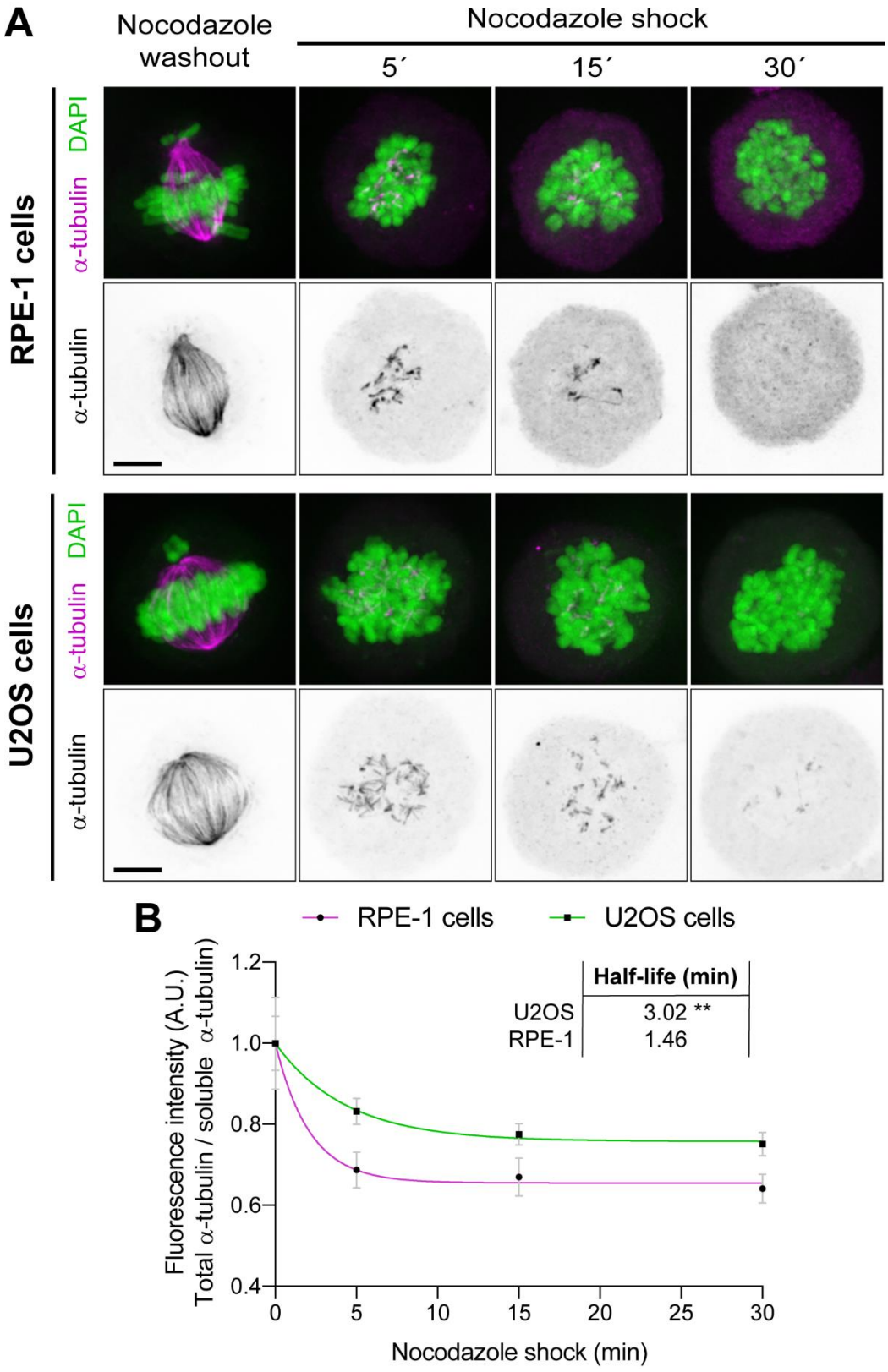

Figure S7. Misaligned chromosomes in chromosomally unstable cancer cells have hyper-stabilized kinetochore-microtubule attachments, related to Figure 7.

a) Representative immunofluorescence images of RPE-1 and U2OS cells stained for

DNA (green) and α-tubulin (magenta). RPE-1 and U2OS cells upon nocodazole treatment and washout to generate misaligned chromosomes were processed for immunofluorescence microscopy after a subsequent nocodazole shock 5, 15 and 30 min after drug addition. Representative immunofluorescence images of the mitotic spindle at each stage are shown. Images are maximum intensity projections of deconvolved z-stacks. Scale bar = 5 µm. **b)** Normalized α-tubulin fluorescence intensity at indicated time points in RPE-1 and U2OS cells after nocodazole shock. Fluorescence intensities were normalized to the levels at time = 0. Data represent mean ± s.d., U2OS n=22 cells, RPE-1 n=22 cells, from 2 independent experiments. Whole lines show single exponential fitting curve (**p≤0.01, extra sum-of-squares F test).

Supplemental References

S1. DeLuca, J.G., Moree, B., Hickey, J.M., Kilmartin, J.V., and Salmon, E.D. (2002). hNuf2 inhibition blocks stable kinetochore-microtubule attachment and induces mitotic cell death in HeLa cells. J Cell Biol *159*, 549-555. 10.1083/jcb.200208159.

S2. DeLuca, J.G., Dong, Y., Hergert, P., Strauss, J., Hickey, J.M., Salmon, E.D., and McEwen, B.F. (2005). Hec1 and nuf2 are core components of the kinetochore outer plate essential for organizing microtubule attachment sites. Mol Biol Cell *16*, 519-531. 10.1091/mbc.e04-09-0852.

S3. Sundin, L.J., Guimaraes, G.J., and Deluca, J.G. (2011). The NDC80 complex proteins Nuf2 and Hec1 make distinct contributions to kinetochore-microtubule attachment in mitosis. Molecular biology of the cell *22*, 759-768. 10.1091/mbc.E10-08-0671

mbc.E10-08-0671 [pii].

S4. Fremont, S., Gerard, A., Galloux, M., Janvier, K., Karess, R.E., and Berlioz-Torrent, C. (2013). Beclin-1 is required for chromosome congression and proper outer kinetochore assembly. EMBO Rep *14*, 364-372. 10.1038/embor.2013.23.

S5. Tanenbaum, M.E., Galjart, N., van Vugt, M.A., and Medema, R.H. (2006). CLIP-170 facilitates the formation of kinetochore-microtubule attachments. EMBO J *25*, 45-57. 10.1038/sj.emboj.7600916.

S6. Amin, M.A., Kobayashi, K., and Tanaka, K. (2015). CLIP-170 tethers kinetochores to microtubule plus ends against poleward force by dynein for

stable kinetochore-microtubule attachment. FEBS Lett *589*, 2739-2746. 10.1016/j.febslet.2015.07.036.

S7. Ritchie, K., Seah, C., Moulin, J., Isaac, C., Dick, F., and Berube, N.G. (2008). Loss of ATRX leads to chromosome cohesion and congression defects. J Cell Biol *180*, 315-324. 10.1083/jcb.200706083.

S8. Archinti, M., Lacasa, C., Teixido-Travesa, N., and Luders, J. (2010). SPICE--a previously uncharacterized protein required for centriole duplication and mitotic chromosome congression. J Cell Sci *123*, 3039-3046. 10.1242/jcs.069963.

S9. Deretic, J., Kerr, A., and Welburn, J.P.I. (2019). A rapid computational approach identifies SPICE1 as an Aurora kinase substrate. Mol Biol Cell *30*, 312-323. 10.1091/mbc.E18-08-0495.

S10. Santamaria, A., Nagel, S., Sillje, H.H.W., and Nigg, E.A. (2008). The spindle protein CHICA mediates localization of the chromokinesin Kid to the mitotic spindle. Curr Biol *18*, 723-729. 10.1016/j.cub.2008.04.041.

S11. Dunsch, A.K., Hammond, D., Lloyd, J., Schermelleh, L., Gruneberg, U., and Barr, F.A. (2012). Dynein light chain 1 and a spindle-associated adaptor promote dynein asymmetry and spindle orientation. The Journal of cell biology *198*, 1039-1054. 10.1083/jcb.201202112.

S12. Wang, L., Zhu, G., Yang, D., Li, Q., Li, Y., Xu, X., He, D., and Zeng, C. (2008). The spindle function of CDCA4. Cell motility and the cytoskeleton *65*, 581-593. 10.1002/cm.20286.

S13. Jang, C.Y., Wong, J., Coppinger, J.A., Seki, A., Yates, J.R., 3rd, and Fang, G. (2008). DDA3 recruits microtubule depolymerase Kif2a to spindle poles and controls spindle dynamics and mitotic chromosome movement. J Cell Biol *181*, 255-267. 10.1083/jcb.200711032.

S14. Ganem, N.J., and Compton, D.A. (2004). The KinI kinesin Kif2a is required for bipolar spindle assembly through a functional relationship with MCAK. J Cell Biol *166*, 473-478. 10.1083/jcb.200404012.

S15. Park, S.J. (2010). Huntingtin-interacting protein 1-related is required for accurate congression and segregation of chromosomes. BMB Rep *43*, 795-800. 10.5483/BMBRep.2010.43.12.795.

S16. Amin, M.A., Matsunaga, S., Uchiyama, S., and Fukui, K. (2008). Nucleophosmin is required for chromosome congression, proper mitotic spindle formation, and kinetochore-microtubule attachment in HeLa cells. FEBS Lett *582*, 3839-3844. 10.1016/j.febslet.2008.10.023.

S17. Holt, S.V., Vergnolle, M.A., Hussein, D., Wozniak, M.J., Allan, V.J., and Taylor, S.S. (2005). Silencing Cenp-F weakens centromeric cohesion, prevents chromosome alignment and activates the spindle checkpoint. Journal of cell science *118*, 4889-4900. 118/20/4889 [pii]

10.1242/jcs.02614.

S18. Yang, Z., Guo, J., Chen, Q., Ding, C., Du, J., and Zhu, X. (2005). Silencing mitosin induces misaligned chromosomes, premature chromosome decondensation before anaphase onset, and mitotic cell death. Mol Cell Biol *25*, 4062-4074. 10.1128/MCB.25.10.4062-4074.2005.

S19. Nishino, M., Kurasawa, Y., Evans, R., Lin, S.H., Brinkley, B.R., and Yu-Lee, L.Y. (2006). NudC is required for Plk1 targeting to the kinetochore and chromosome congression. Curr Biol *16*, 1414-1421. 10.1016/j.cub.2006.05.052.

S20. Chuang, C., Pan, J., Hawke, D.H., Lin, S.H., and Yu-Lee, L.Y. (2013). NudC deacetylation regulates mitotic progression. PLoS One *8*, e73841. 10.1371/journal.pone.0073841.

S21. Gambe, A.E., Matsunaga, S., Takata, H., Ono-Maniwa, R., Baba, A., Uchiyama, S., and Fukui, K. (2009). A nucleolar protein RRS1 contributes to chromosome congression. FEBS Lett *583*, 1951-1956. 10.1016/j.febslet.2009.05.033.

S22. Zhang, L., Iyer, J., Chowdhury, A., Ji, M., Xiao, L., Yang, S., Chen, Y., Tsai, M.Y., and Dong, J. (2012). KIBRA regulates aurora kinase activity and is required for precise chromosome alignment during mitosis. J Biol Chem *287*, 34069-34077. 10.1074/jbc.M112.385518.

S23. Ma, N., Matsunaga, S., Takata, H., Ono-Maniwa, R., Uchiyama, S., and Fukui, K. (2007). Nucleolin functions in nucleolus formation and chromosome congression. Journal of cell science *120*, 2091-2105. 10.1242/jcs.008771.

S24. Li, N., Yuan, K., Yan, F., Huo, Y., Zhu, T., Liu, X., Guo, Z., and Yao, X. (2009). PinX1 is recruited to the mitotic chromosome periphery by Nucleolin and facilitates chromosome congression. Biochem Biophys Res Commun *384*, 76-81. 10.1016/j.bbrc.2009.04.077.

S25. Jang, C.Y., Coppinger, J.A., Yates, J.R., 3rd, and Fang, G. (2010). Phospho-regulation of DDA3 function in mitosis. Biochem Biophys Res Commun *393*, 259-263. 10.1016/j.bbrc.2010.01.115.

S26. Jang, C.Y., Coppinger, J.A., Yates, J.R., 3rd, and Fang, G. (2011). Mitotic kinases regulate MT-polymerizing/MT-bundling activity of DDA3. Biochem Biophys Res Commun *408*, 174-179. 10.1016/j.bbrc.2011.04.004.

S27. Jang, C.Y., and Fang, G. (2011). DDA3 associates with MCAK and controls chromosome congression. Biochem Biophys Res Commun *407*, 610-614. 10.1016/j.bbrc.2011.03.081.

S28. Park, J.E., Song, H., Kwon, H.J., and Jang, C.Y. (2016). Ska1 cooperates with DDA3 for spindle dynamics and spindle attachment to kinetochore. Biochem Biophys Res Commun *470*, 586-592. 10.1016/j.bbrc.2016.01.101.

S29. Johnson, V.L., Scott, M.I., Holt, S.V., Hussein, D., and Taylor, S.S. (2004). Bub1 is required for kinetochore localization of BubR1, Cenp-E, Cenp-F and Mad2, and chromosome congression. Journal of cell science *117*, 1577-1589. 10.1242/jcs.01006

117/8/1577 [pii].

S30. Morrow, C.J., Tighe, A., Johnson, V.L., Scott, M.I., Ditchfield, C., and Taylor, S.S. (2005). Bub1 and aurora B cooperate to maintain BubR1-mediated inhibition of APC/CCdc20. J Cell Sci *118*, 3639-3652. 10.1242/jcs.02487.

S31. Meraldi, P., and Sorger, P.K. (2005). A dual role for Bub1 in the spindle checkpoint and chromosome congression. The EMBO journal *24*, 1621-1633. 7600641 [pii]

10.1038/sj.emboj.7600641.

S32. Ditchfield, C., Johnson, V.L., Tighe, A., Ellston, R., Haworth, C., Johnson, T., Mortlock, A., Keen, N., and Taylor, S.S. (2003). Aurora B couples chromosome alignment with anaphase by targeting BubR1, Mad2, and Cenp-E to kinetochores. J Cell Biol *161*, 267-280. 10.1083/jcb.200208091.

S33. Lampson, M.A., and Kapoor, T.M. (2005). The human mitotic checkpoint protein BubR1 regulates chromosome-spindle attachments. Nat Cell Biol *7*, 93-98. 10.1038/ncb1208.

S34. Raaijmakers, J.A., Tanenbaum, M.E., Maia, A.F., and Medema, R.H. (2009). RAMA1 is a novel kinetochore protein involved in kinetochore-microtubule attachment. J Cell Sci *122*, 2436-2445. 10.1242/jcs.051912.

S35. Gaitanos, T.N., Santamaria, A., Jeyaprakash, A.A., Wang, B., Conti, E., and Nigg, E.A. (2009). Stable kinetochore-microtubule interactions depend on the Ska complex and its new component Ska3/C13Orf3. EMBO J *28*, 1442-1452. 10.1038/emboj.2009.96.

S36. Daum, J.R., Wren, J.D., Daniel, J.J., Sivakumar, S., McAvoy, J.N., Potapova, T.A., and Gorbsky, G.J. (2009). Ska3 is required for spindle checkpoint silencing and the maintenance of chromosome cohesion in mitosis. Curr Biol *19*, 1467-1472. 10.1016/j.cub.2009.07.017.

S37. Sivakumar, S., Daum, J.R., Tipton, A.R., Rankin, S., and Gorbsky, G.J. (2014). The spindle and kinetochore-associated (Ska) complex enhances binding of the anaphase-promoting complex/cyclosome (APC/C) to chromosomes and promotes mitotic exit. Molecular biology of the cell *25*, 594-605. 10.1091/mbc.E13-07-0421.

S38. Welburn, J.P., Grishchuk, E.L., Backer, C.B., Wilson-Kubalek, E.M., Yates, J.R., 3rd, and Cheeseman, I.M. (2009). The human kinetochore Ska1 complex facilitates microtubule depolymerization-coupled motility. Dev Cell *16*, 374-385. 10.1016/j.devcel.2009.01.011.

S39. Garrett, S., Auer, K., Compton, D.A., and Kapoor, T.M. (2002). hTPX2 is required for normal spindle morphology and centrosome integrity during vertebrate cell division. Curr Biol *12*, 2055-2059. 10.1016/s0960-9822(02)01277-0.

S40. Goshima, G. (2011). Identification of a TPX2-like microtubule-associated protein in Drosophila. PLoS One *6*, e28120. 10.1371/journal.pone.0028120.

S41. Itoh, G., Sugino, S., Ikeda, M., Mizuguchi, M., Kanno, S., Amin, M.A., Iemura, K., Yasui, A., Hirota, T., and Tanaka, K. (2013). Nucleoporin Nup188 is required for chromosome alignment in mitosis. Cancer Sci *104*, 871-879. 10.1111/cas.12159.

S42. Mazumdar, M., Sundareshan, S., and Misteli, T. (2004). Human chromokinesin KIF4A functions in chromosome condensation and segregation. J Cell Biol *166*, 613-620. 10.1083/jcb.200401142.

S43. Yang, Z., Tulu, U.S., Wadsworth, P., and Rieder, C.L. (2007). Kinetochore dynein is required for chromosome motion and congression independent of the spindle checkpoint. Curr Biol *17*, 973-980. 10.1016/j.cub.2007.04.056.

S44. Li, Y., Yu, W., Liang, Y., and Zhu, X. (2007). Kinetochore dynein generates a poleward pulling force to facilitate congression and full chromosome alignment. Cell Res *17*, 701-712. 10.1038/cr.2007.65.

S45. McHedlishvili, N., Wieser, S., Holtackers, R., Mouysset, J., Belwal, M., Amaro, A.C., and Meraldi, P. (2012). Kinetochores accelerate centrosome separation to ensure faithful chromosome segregation. J Cell Sci *125*, 906-918. 10.1242/jcs.091967.

S46. Raemaekers, T., Ribbeck, K., Beaudouin, J., Annaert, W., Van Camp, M., Stockmans, I., Smets, N., Bouillon, R., Ellenberg, J., and Carmeliet, G. (2003). NuSAP, a novel microtubule-associated protein involved in mitotic spindle organization. J Cell Biol *162*, 1017-1029. 10.1083/jcb.200302129.

S47. Li, C., Xue, C., Yang, Q., Low, B.C., and Liou, Y.C. (2016). NuSAP governs chromosome oscillation by facilitating the Kid-generated polar ejection force. Nat Commun *7*, 10597. 10.1038/ncomms10597.

S48. Ma, N., Matsunaga, S., Morimoto, A., Sakashita, G., Urano, T., Uchiyama, S., and Fukui, K. (2011). The nuclear scaffold protein SAF-A is required for kinetochore-microtubule attachment and contributes to the targeting of Aurora-A to mitotic spindles. J Cell Sci *124*, 394-404. 10.1242/jcs.063347.

S49. Yang, S., Liu, X., Yin, Y., Fukuda, M.N., and Zhou, J. (2008). Tastin is required for bipolar spindle assembly and centrosome integrity during mitosis. FASEB J *22*, 1960-1972. 10.1096/fj.07-081463.

S50. Dynek, J.N., and Smith, S. (2004). Resolution of sister telomere association is required for progression through mitosis. Science *304*, 97-100. 10.1126/science.1094754.

S51. Chang, P., Coughlin, M., and Mitchison, T.J. (2005). Tankyrase-1 polymerization of poly(ADP-ribose) is required for spindle structure and function. Nat Cell Biol *7*, 1133-1139. 10.1038/ncb1322.

S52. Hanisch, A., Sillje, H.H., and Nigg, E.A. (2006). Timely anaphase onset requires a novel spindle and kinetochore complex comprising Ska1 and Ska2. EMBO J *25*, 5504-5515. 10.1038/sj.emboj.7601426.

S53. Auckland, P., Clarke, N.I., Royle, S.J., and McAinsh, A.D. (2017). Congressing kinetochores progressively load Ska complexes to prevent force-dependent detachment. J Cell Biol *216*, 1623-1639. 10.1083/jcb.201607096.

S54. Sillje, H.H., Nagel, S., Korner, R., and Nigg, E.A. (2006). HURP is a Ran-importin beta-regulated protein that stabilizes kinetochore microtubules in the vicinity of chromosomes. Curr Biol *16*, 731-742. 10.1016/j.cub.2006.02.070.

S55. Wong, J., and Fang, G. (2006). HURP controls spindle dynamics to promote proper interkinetochore tension and efficient kinetochore capture. The Journal of cell biology *173*, 879-891. 10.1083/jcb.200511132.

S56. Ye, F., Tan, L., Yang, Q., Xia, Y., Deng, L.W., Murata-Hori, M., and Liou, Y.C. (2011). HURP regulates chromosome congression by modulating kinesin Kif18A function. Curr Biol *21*, 1584-1591. 10.1016/j.cub.2011.08.024.

S57. Zhang, Y., Tan, L., Yang, Q., Li, C., and Liou, Y.C. (2018). The microtubule-associated protein HURP recruits the centrosomal protein TACC3 to regulate K-fiber formation and support chromosome congression. J Biol Chem *293*, 15733-15747. 10.1074/jbc.RA118.003676.

S58. Nakamura, A., Arai, H., and Fujita, N. (2009). Centrosomal Aki1 and cohesin function in separase-regulated centriole disengagement. J Cell Biol *187*, 607-614. 10.1083/jcb.200906019.

S59. Krauss, S.W., Spence, J.R., Bahmanyar, S., Barth, A.I., Go, M.M., Czerwinski, D., and Meyer, A.J. (2008). Downregulation of protein 4.1R, a mature centriole protein, disrupts centrosomes, alters cell cycle progression, and perturbs mitotic spindles and anaphase. Mol Cell Biol *28*, 2283-2294. 10.1128/MCB.02021-07.

S60. Wu, G., Lin, Y.T., Wei, R., Chen, Y., Shan, Z., and Lee, W.H. (2008). Hice1, a novel microtubule-associated protein required for maintenance of spindle integrity and chromosomal stability in human cells. Mol Cell Biol *28*, 3652-3662. 10.1128/MCB.01923-07.

S61. Lawo, S., Bashkurov, M., Mullin, M., Ferreria, M.G., Kittler, R., Habermann, B., Tagliaferro, A., Poser, I., Hutchins, J.R., Hegemann, B., et al. (2009). HAUS,

the 8-subunit human Augmin complex, regulates centrosome and spindle integrity. Curr Biol *19*, 816-826. 10.1016/j.cub.2009.04.033.

S62. Huang, Y., Yao, Y., Xu, H.Z., Wang, Z.G., Lu, L., and Dai, W. (2009). Defects in chromosome congression and mitotic progression in KIF18A-deficient cells are partly mediated through impaired functions of CENP-E. Cell Cycle *8*, 2643-2649. 10.4161/cc.8.16.9366.

S63. Stumpff, J., von Dassow, G., Wagenbach, M., Asbury, C., and Wordeman, L. (2008). The kinesin-8 motor Kif18A suppresses kinetochore movements to control mitotic chromosome alignment. Dev Cell *14*, 252-262. 10.1016/j.devcel.2007.11.014.

S64. Liu, X.S., Zhao, X.D., Wang, X., Yao, Y.X., Zhang, L.L., Shu, R.Z., Ren, W.H., Huang, Y., Huang, L., Gu, M.M., et al. (2010). Germinal Cell Aplasia in Kif18a Mutant Male Mice Due to Impaired Chromosome Congression and Dysregulated BubR1 and CENP-E. Genes & cancer *1*, 26-39. 10.1177/1947601909358184.

S65. Stumpff, J., Wagenbach, M., Franck, A., Asbury, C.L., and Wordeman, L. (2012). Kif18A and chromokinesins confine centromere movements via microtubule growth suppression and spatial control of kinetochore tension. Dev Cell *22*, 1017-1029. 10.1016/j.devcel.2012.02.013.

S66. Mayr, M.I., Hummer, S., Bormann, J., Gruner, T., Adio, S., Woehlke, G., and Mayer, T.U. (2007). The human kinesin Kif18A is a motile microtubule depolymerase essential for chromosome congression. Curr Biol *17*, 488-498. 10.1016/j.cub.2007.02.036.

S67. Fonseca, C.L., Malaby, H.L.H., Sepaniac, L.A., Martin, W., Byers, C., Czechanski, A., Messinger, D., Tang, M., Ohi, R., Reinholdt, L.G., and Stumpff,

J. (2019). Mitotic chromosome alignment ensures mitotic fidelity by promoting interchromosomal compaction during anaphase. The Journal of cell biology *218*, 1148-1163. 10.1083/jcb.201807228.

S68. Kimura, M., Yoshioka, T., Saio, M., Banno, Y., Nagaoka, H., and Okano, Y. (2013). Mitotic catastrophe and cell death induced by depletion of centrosomal proteins. Cell Death Dis *4*, e603. 10.1038/cddis.2013.108.

S69. Schneider, L., Essmann, F., Kletke, A., Rio, P., Hanenberg, H., Wetzel, W., Schulze-Osthoff, K., Nurnberg, B., and Piekorz, R.P. (2007). The transforming acidic coiled coil 3 protein is essential for spindle-dependent chromosome alignment and mitotic survival. J Biol Chem *282*, 29273-29283. 10.1074/jbc.M704151200.

S70. Lin, C.H., Hu, C.K., and Shih, H.M. (2010). Clathrin heavy chain mediates TACC3 targeting to mitotic spindles to ensure spindle stability. The Journal of cell biology *189*, 1097-1105. 10.1083/jcb.200911120.

S71. Cheeseman, L.P., Harry, E.F., McAinsh, A.D., Prior, I.A., and Royle, S.J. (2013). Specific removal of TACC3-ch-TOG-clathrin at metaphase deregulates kinetochore fiber tension. J Cell Sci *126*, 2102-2113. 10.1242/jcs.124834.

S72. Gergely, F., Draviam, V.M., and Raff, J.W. (2003). The ch-TOG/XMAP215 protein is essential for spindle pole organization in human somatic cells. Genes Dev *17*, 336-341. 10.1101/gad.245603.

S73. Muto, Y., Yoshioka, T., Kimura, M., Matsunami, M., Saya, H., and Okano, Y. (2008). An evolutionarily conserved leucine-rich repeat protein CLERC is a centrosomal protein required for spindle pole integrity. Cell Cycle *7*, 2738-2748. 10.4161/cc.7.17.6591.

S74. Oshimori, N., Ohsugi, M., and Yamamoto, T. (2006). The Plk1 target Kizuna stabilizes mitotic centrosomes to ensure spindle bipolarity. Nat Cell Biol *8*, 1095-1101. 10.1038/ncb1474.

S75. Fielding, A.B., Dobreva, I., McDonald, P.C., Foster, L.J., and Dedhar, S. (2008). Integrin-linked kinase localizes to the centrosome and regulates mitotic spindle organization. J Cell Biol *180*, 681-689. 10.1083/jcb.200710074.

S76. Dunsch, A.K., Linnane, E., Barr, F.A., and Gruneberg, U. (2011). The astrin-kinastrin/SKAP complex localizes to microtubule plus ends and facilitates chromosome alignment. The Journal of cell biology *192*, 959-968. 10.1083/jcb.201008023.

S77. Schmidt, J.C., Kiyomitsu, T., Hori, T., Backer, C.B., Fukagawa, T., and Cheeseman, I.M. (2010). Aurora B kinase controls the targeting of the Astrin-SKAP complex to bioriented kinetochores. J Cell Biol *191*, 269-280. 10.1083/jcb.201006129.

S78. Fang, L., Seki, A., and Fang, G. (2009). SKAP associates with kinetochores and promotes the metaphase-to-anaphase transition. Cell Cycle *8*, 2819-2827. 10.4161/cc.8.17.9514.

S79. Huang, Y., Wang, W., Yao, P., Wang, X., Liu, X., Zhuang, X., Yan, F., Zhou, J., Du, J., Ward, T., et al. (2012). CENP-E kinesin interacts with SKAP protein to orchestrate accurate chromosome segregation in mitosis. J Biol Chem *287*, 1500-1509. 10.1074/jbc.M111.277194.

S80. Logarinho, E., Maffini, S., Barisic, M., Marques, A., Toso, A., Meraldi, P., and Maiato, H. (2012). CLASPs prevent irreversible multipolarity by ensuring spindle-pole resistance to traction forces during chromosome alignment. Nat Cell Biol *14*, 295-303. 10.1038/ncb2423.

S81. Haren, L., Gnadt, N., Wright, M., and Merdes, A. (2009). NuMA is required for proper spindle assembly and chromosome alignment in prometaphase. BMC Res Notes *2*, 64. 10.1186/1756-0500-2-64.

S82. Iwakiri, Y., Kamakura, S., Hayase, J., and Sumimoto, H. (2013). Interaction of NuMA protein with the kinesin Eg5: its possible role in bipolar spindle assembly and chromosome alignment. Biochem J *451*, 195-204. 10.1042/BJ20121447.

S83. Wong, R.W., Blobel, G., and Coutavas, E. (2006). Rae1 interaction with NuMA is required for bipolar spindle formation. Proc Natl Acad Sci U S A *103*, 19783-19787. 10.1073/pnas.0609582104.

S84. Blower, M.D., Nachury, M., Heald, R., and Weis, K. (2005). A Rae1-containing ribonucleoprotein complex is required for mitotic spindle assembly. Cell *121*, 223-234. 10.1016/j.cell.2005.02.016.

S85. Joseph, J., Liu, S.T., Jablonski, S.A., Yen, T.J., and Dasso, M. (2004). The RanGAP1-RanBP2 complex is essential for microtubule-kinetochore interactions in vivo. Curr Biol *14*, 611-617. 10.1016/j.cub.2004.03.031.

S86. Barisic, M., Sohm, B., Mikolcevic, P., Wandke, C., Rauch, V., Ringer, T., Hess, M., Bonn, G., and Geley, S. (2010). Spindly/CCDC99 is required for efficient chromosome congression and mitotic checkpoint regulation. Molecular biology of the cell *21*, 1968-1981. 10.1091/mbc.E09-04-0356

E09-04-0356 [pii].

S87. Raaijmakers, J.A., Tanenbaum, M.E., and Medema, R.H. (2013). Systematic dissection of dynein regulators in mitosis. The Journal of cell biology *201*, 201-215. 10.1083/jcb.201208098.

S88. Torres, J.Z., Summers, M.K., Peterson, D., Brauer, M.J., Lee, J., Senese, S., Gholkar, A.A., Lo, Y.C., Lei, X., Jung, K., et al. (2011). The STARD9/Kif16a

kinesin associates with mitotic microtubules and regulates spindle pole assembly. Cell *147*, 1309-1323. 10.1016/j.cell.2011.11.020.

S89. Holmfeldt, P., Zhang, X., Stenmark, S., Walczak, C.E., and Gullberg, M. (2005). CaMKIIgamma-mediated inactivation of the Kin I kinesin MCAK is essential for bipolar spindle formation. EMBO J *24*, 1256-1266. 10.1038/sj.emboj.7600601.

S90. Maia, A.F., Feijao, T., Vromans, M.J., Sunkel, C.E., and Lens, S.M. (2010). Aurora B kinase cooperates with CENP-E to promote timely anaphase onset. Chromosoma *119*, 405-413. 10.1007/s00412-010-0265-x.

S91. Stevens, D., Gassmann, R., Oegema, K., and Desai, A. (2011). Uncoordinated loss of chromatid cohesion is a common outcome of extended metaphase arrest. PLoS One *6*, e22969. 10.1371/journal.pone.0022969.

S92. Tanudji, M., Shoemaker, J., L'Italien, L., Russell, L., Chin, G., and Schebye, X.M. (2004). Gene silencing of CENP-E by small interfering RNA in HeLa cells leads to missegregation of chromosomes after a mitotic delay. Molecular biology of the cell *15*, 3771-3781. 10.1091/mbc.e03-07-0482.

S93. Barisic, M., Aguiar, P., Geley, S., and Maiato, H. (2014). Kinetochore motors drive congression of peripheral polar chromosomes by overcoming random arm-ejection forces. Nat Cell Biol *16*, 1249-1256. 10.1038/ncb3060.

S94. Royle, S.J., Bright, N.A., and Lagnado, L. (2005). Clathrin is required for the function of the mitotic spindle. Nature *434*, 1152-1157. 10.1038/nature03502.

S95. Foraker, A.B., Camus, S.M., Evans, T.M., Majeed, S.R., Chen, C.Y., Taner, S.B., Correa, I.R., Jr., Doxsey, S.J., and Brodsky, F.M. (2012). Clathrin promotes centrosome integrity in early mitosis through stabilization of centrosomal ch-TOG. The Journal of cell biology *198*, 591-605. 10.1083/jcb.201205116.

S96. Oshimori, N., Li, X., Ohsugi, M., and Yamamoto, T. (2009). Cep72 regulates the localization of key centrosomal proteins and proper bipolar spindle formation. The EMBO journal *28*, 2066-2076. 10.1038/emboj.2009.161.

S97. Kim, K., and Rhee, K. (2011). The pericentriolar satellite protein CEP90 is crucial for integrity of the mitotic spindle pole. Journal of cell science *124*, 338-347. 10.1242/jcs.078329.

S98. Mimori-Kiyosue, Y., Grigoriev, I., Lansbergen, G., Sasaki, H., Matsui, C., Severin, F., Galjart, N., Grosveld, F., Vorobjev, I., Tsukita, S., and Akhmanova, A. (2005). CLASP1 and CLASP2 bind to EB1 and regulate microtubule plus-end dynamics at the cell cortex. J Cell Biol *168*, 141-153. 10.1083/jcb.200405094.

S99. Girao, H., Okada, N., Rodrigues, T.A., Silva, A.O., Figueiredo, A.C., Garcia, Z., Moutinho-Santos, T., Hayashi, I., Azevedo, J.E., Macedo-Ribeiro, S., and Maiato, H. (2020). CLASP2 binding to curved microtubule tips promotes flux and stabilizes kinetochore attachments. J Cell Biol *219*. 10.1083/jcb.201905080.

S100. Maiato, H., Rieder, C.L., Earnshaw, W.C., and Sunkel, C.E. (2003). How do kinetochores CLASP dynamic microtubules? Cell Cycle *2*, 511-514. 10.4161/cc.2.6.576.

S101. Fuller, B.G., Lampson, M.A., Foley, E.A., Rosasco-Nitcher, S., Le, K.V., Tobelmann, P., Brautigan, D.L., Stukenberg, P.T., and Kapoor, T.M. (2008). Midzone activation of aurora B in anaphase produces an intracellular phosphorylation gradient. Nature *453*, 1132-1136. 10.1038/nature06923.

S102. Hauf, S., Cole, R.W., LaTerra, S., Zimmer, C., Schnapp, G., Walter, R., Heckel, A., van Meel, J., Rieder, C.L., and Peters, J.M. (2003). The small molecule

Hesperadin reveals a role for Aurora B in correcting kinetochore-microtubule attachment and in maintaining the spindle assembly checkpoint. J Cell Biol *161*, 281-294. 10.1083/jcb.200208092.

S103. Hegarat, N., Smith, E., Nayak, G., Takeda, S., Eyers, P.A., and Hochegger, H. (2011). Aurora A and Aurora B jointly coordinate chromosome segregation and anaphase microtubule dynamics. J Cell Biol *195*, 1103-1113. 10.1083/jcb.201105058.

S104. Thein, K.H., Kleylein-Sohn, J., Nigg, E.A., and Gruneberg, U. (2007). Astrin is required for the maintenance of sister chromatid cohesion and centrosome integrity. J Cell Biol *178*, 345-354. 10.1083/jcb.200701163.

S105. Hoar, K., Chakravarty, A., Rabino, C., Wysong, D., Bowman, D., Roy, N., and Ecsedy, J.A. (2007). MLN8054, a small-molecule inhibitor of Aurora A, causes spindle pole and chromosome congression defects leading to aneuploidy. Mol Cell Biol *27*, 4513-4525. 10.1128/MCB.02364-06.

S106. Sasai, K., Parant, J.M., Brandt, M.E., Carter, J., Adams, H.P., Stass, S.A., Killary, A.M., Katayama, H., and Sen, S. (2008). Targeted disruption of Aurora A causes abnormal mitotic spindle assembly, chromosome misalignment and embryonic lethality. Oncogene *27*, 4122-4127. 10.1038/onc.2008.47.

S107. De Luca, M., Lavia, P., and Guarguaglini, G. (2006). A functional interplay between Aurora-A, Plk1 and TPX2 at spindle poles: Plk1 controls centrosomal localization of Aurora-A and TPX2 spindle association. Cell Cycle *5*, 296-303. 10.4161/cc.5.3.2392.

S108. De Luca, M., Brunetto, L., Asteriti, I.A., Giubettini, M., Lavia, P., and Guarguaglini, G. (2008). Aurora-A and ch-TOG act in a common pathway in

control of spindle pole integrity. Oncogene *27*, 6539-6549. 10.1038/onc.2008.252.

S109. Mackay, A.M., Ainsztein, A.M., Eckley, D.M., and Earnshaw, W.C. (1998). A dominant mutant of inner centromere protein (INCENP), a chromosomal protein, disrupts prometaphase congression and cytokinesis. J Cell Biol *140*, 991-1002. 10.1083/jcb.140.5.991.

S110. Xu, Z., Ogawa, H., Vagnarelli, P., Bergmann, J.H., Hudson, D.F., Ruchaud, S., Fukagawa, T., Earnshaw, W.C., and Samejima, K. (2009). INCENP-aurora B interactions modulate kinase activity and chromosome passenger complex localization. The Journal of cell biology *187*, 637-653. 10.1083/jcb.200906053.

S111. Dai, J., Sultan, S., Taylor, S.S., and Higgins, J.M. (2005). The kinase haspin is required for mitotic histone H3 Thr 3 phosphorylation and normal metaphase chromosome alignment. Genes & development *19*, 472-488. 10.1101/gad.1267105.

S112. Dai, J., Kateneva, A.V., and Higgins, J.M. (2009). Studies of haspin-depleted cells reveal that spindle-pole integrity in mitosis requires chromosome cohesion. J Cell Sci *122*, 4168-4176. 10.1242/jcs.054122.

S113. Xu, P., Virshup, D.M., and Lee, S.H. (2014). B56-PP2A regulates motor dynamics for mitotic chromosome alignment. J Cell Sci *127*, 4567-4573. 10.1242/jcs.154609.

S114. Bharadwaj, R., Qi, W., and Yu, H. (2004). Identification of two novel components of the human NDC80 kinetochore complex. J Biol Chem *279*, 13076-13085. 10.1074/jbc.M310224200.

S115. McCleland, M.L., Kallio, M.J., Barrett-Wilt, G.A., Kestner, C.A., Shabanowitz, J., Hunt, D.F., Gorbsky, G.J., and Stukenberg, P.T. (2004). The vertebrate

Ndc80 complex contains Spc24 and Spc25 homologs, which are required to establish and maintain kinetochore-microtubule attachment. Curr Biol *14*, 131-137. 10.1016/j.cub.2003.12.058.

S116. Lo, K.W., Kogoy, J.M., and Pfister, K.K. (2007). The DYNLT3 light chain directly links cytoplasmic dynein to a spindle checkpoint protein, Bub3. J Biol Chem *282*, 11205-11212. 10.1074/jbc.M611279200.

S117. Vergnolle, M.A., and Taylor, S.S. (2007). Cenp-F links kinetochores to Ndel1/Nde1/Lis1/dynein microtubule motor complexes. Curr Biol *17*, 1173-1179. 10.1016/j.cub.2007.05.077.

S118. Moon, H.M., Youn, Y.H., Pemble, H., Yingling, J., Wittmann, T., and Wynshaw-Boris, A. (2014). LIS1 controls mitosis and mitotic spindle organization via the LIS1-NDEL1-dynein complex. Hum Mol Genet *23*, 449-466. 10.1093/hmg/ddt436.

S119. Auckland, P., and McAinsh, A.D. (2015). Building an integrated model of chromosome congression. J Cell Sci *128*, 3363-3374. 10.1242/jcs.169367.

S120. Horgan, C.P., Hanscom, S.R., and McCaffrey, M.W. (2011). Dynein LIC1 localizes to the mitotic spindle and midbody and LIC2 localizes to spindle poles during cell division. Cell Biol Int *35*, 171-178. 10.1042/CBI20100284.

S121. Einarson, M.B., Cukierman, E., Compton, D.A., and Golemis, E.A. (2004). Human enhancer of invasion-cluster, a coiled-coil protein required for passage through mitosis. Mol Cell Biol *24*, 3957-3971. 10.1128/MCB.24.9.3957-3971.2004.

S122. Lens, S.M., Wolthuis, R.M., Klompmaker, R., Kauw, J., Agami, R., Brummelkamp, T., Kops, G., and Medema, R.H. (2003). Survivin is required for

a sustained spindle checkpoint arrest in response to lack of tension. EMBO J *22*, 2934-2947. 10.1093/emboj/cdg307.

S123. Carvalho, A., Carmena, M., Sambade, C., Earnshaw, W.C., and Wheatley, S.P. (2003). Survivin is required for stable checkpoint activation in taxol-treated HeLa cells. J Cell Sci *116*, 2987-2998. 10.1242/jcs.00612.

S124. Uren, A.G., Wong, L., Pakusch, M., Fowler, K.J., Burrows, F.J., Vaux, D.L., and Choo, K.H. (2000). Survivin and the inner centromere protein INCENP show similar cell-cycle localization and gene knockout phenotype. Curr Biol *10*, 1319-1328. 10.1016/s0960-9822(00)00769-7.

S125. Cho, J.H., Chang, C.J., Chen, C.Y., and Tang, T.K. (2006). Depletion of CPAP by RNAi disrupts centrosome integrity and induces multipolar spindles. Biochem Biophys Res Commun *339*, 742-747. 10.1016/j.bbrc.2005.11.074.

S126. Martin-Lluesma, S., Stucke, V.M., and Nigg, E.A. (2002). Role of Hec1 in spindle checkpoint signaling and kinetochore recruitment of Mad1/Mad2. Science *297*, 2267-2270. 10.1126/science.1075596.

S127. Li, L., Yang, L., Scudiero, D.A., Miller, S.A., Yu, Z.X., Stukenberg, P.T., Shoemaker, R.H., and Kotin, R.M. (2007). Development of recombinant adeno-associated virus vectors carrying small interfering RNA (shHec1)-mediated depletion of kinetochore Hec1 protein in tumor cells. Gene Ther *14*, 814-827. 10.1038/sj.gt.3302933.

S128. Lee, M.H., Lin, L., Equilibrina, I., Uchiyama, S., Matsunaga, S., and Fukui, K. (2011). ASURA (PHB2) Is Required for Kinetochore Assembly and Subsequent Chromosome Congression. Acta Histochem Cytochem *44*, 247-258. 10.1267/ahc.11033.

S129. Gassmann, R., Carvalho, A., Henzing, A.J., Ruchaud, S., Hudson, D.F., Honda, R., Nigg, E.A., Gerloff, D.L., and Earnshaw, W.C. (2004). Borealin: a novel chromosomal passenger required for stability of the bipolar mitotic spindle. J Cell Biol *166*, 179-191. 10.1083/jcb.200404001.

S130. Beauchene, N.A., Diaz-Martinez, L.A., Furniss, K., Hsu, W.S., Tsai, H.J., Chamberlain, C., Esponda, P., Gimenez-Abian, J.F., and Clarke, D.J. (2010). Rad21 is required for centrosome integrity in human cells independently of its role in chromosome cohesion. Cell Cycle *9*, 1774-1780. 10.4161/cc.9.9.11524.

S131. Diaz-Martinez, L.A., Beauchene, N.A., Furniss, K., Esponda, P., Gimenez-Abian, J.F., and Clarke, D.J. (2010). Cohesin is needed for bipolar mitosis in human cells. Cell Cycle *9*, 1764-1773. 10.4161/cc.9.9.11525.

S132. Woolner, S., O'Brien, L.L., Wiese, C., and Bement, W.M. (2008). Myosin-10 and actin filaments are essential for mitotic spindle function. J Cell Biol *182*, 77-88. 10.1083/jcb.200804062.

S133. Wang, X., Yang, Y., Duan, Q., Jiang, N., Huang, Y., Darzynkiewicz, Z., and Dai, W. (2008). sSgo1, a major splice variant of Sgo1, functions in centriole cohesion where it is regulated by Plk1. Dev Cell *14*, 331-341. 10.1016/j.devcel.2007.12.007.

S134. McGuinness, B.E., Hirota, T., Kudo, N.R., Peters, J.M., and Nasmyth, K. (2005). Shugoshin prevents dissociation of cohesin from centromeres during mitosis in vertebrate cells. PLoS Biol *3*, e86. 10.1371/journal.pbio.0030086.

S135. McKinley, K.L., Sekulic, N., Guo, L.Y., Tsinman, T., Black, B.E., and Cheeseman, I.M. (2015). The CENP-L-N Complex Forms a Critical Node in an Integrated Meshwork of Interactions at the Centromere-Kinetochore Interface. Mol Cell *60*, 886-898. 10.1016/j.molcel.2015.10.027.

S136. Prendergast, L., van Vuuren, C., Kaczmarczyk, A., Doering, V., Hellwig, D., Quinn, N., Hoischen, C., Diekmann, S., and Sullivan, K.F. (2011). Premitotic assembly of human CENPs -T and -W switches centromeric chromatin to a mitotic state. PLoS Biol *9*, e1001082. 10.1371/journal.pbio.1001082.

S137. Wood, L., Booth, D.G., Vargiu, G., Ohta, S., deLima Alves, F., Samejima, K., Fukagawa, T., Rappsilber, J., and Earnshaw, W.C. (2016). Auxin/AID versus conventional knockouts: distinguishing the roles of CENP-T/W in mitotic kinetochore assembly and stability. Open Biol *6*, 150230. 10.1098/rsob.150230.

S138. Ali, A., Veeranki, S.N., Chinchole, A., and Tyagi, S. (2017). MLL/WDR5 Complex Regulates Kif2A Localization to Ensure Chromosome Congression and Proper Spindle Assembly during Mitosis. Dev Cell *41*, 605-622 e607. 10.1016/j.devcel.2017.05.023.

S139. Chun, Y., Kim, R., and Lee, S. (2016). Centromere Protein (CENP)-W Interacts with Heterogeneous Nuclear Ribonucleoprotein (hnRNP) U and May Contribute to Kinetochore-Microtubule Attachment in Mitotic Cells. PLoS One *11*, e0149127. 10.1371/journal.pone.0149127.

S140. Liu, X., Zheng, H., and Qu, C.K. (2012). Protein tyrosine phosphatase Shp2 (Ptpn11) plays an important role in maintenance of chromosome stability. Cancer Res *72*, 5296-5306. 10.1158/0008-5472.CAN-12-1495.

S141. Takata, H., Matsunaga, S., Morimoto, A., Ma, N., Kurihara, D., Ono-Maniwa, R., Nakagawa, M., Azuma, T., Uchiyama, S., and Fukui, K. (2007). PHB2 protects sister-chromatid cohesion in mitosis. Curr Biol *17*, 1356-1361. 10.1016/j.cub.2007.07.009.

S142. Equilibrina, I., Matsunaga, S., Morimoto, A., Hashimoto, T., Uchiyama, S., and Fukui, K. (2013). ASURA (PHB2) interacts with Scc1 through chromatin. Cytogenet Genome Res *139*, 225-233. 10.1159/000350004.

S143. Orthaus, S., Ohndorf, S., and Diekmann, S. (2006). RNAi knockdown of human kinetochore protein CENP-H. Biochem Biophys Res Commun *348*, 36-46. 10.1016/j.bbrc.2006.06.187.

S144. Amaro, A.C., Samora, C.P., Holtackers, R., Wang, E., Kingston, I.J., Alonso, M., Lampson, M., McAinsh, A.D., and Meraldi, P. (2010). Molecular control of kinetochore-microtubule dynamics and chromosome oscillations. Nat Cell Biol *12*, 319-329. 10.1038/ncb2033.

S145. Carleton, M., Mao, M., Biery, M., Warrener, P., Kim, S., Buser, C., Marshall, C.G., Fernandes, C., Annis, J., and Linsley, P.S. (2006). RNA interference-mediated silencing of mitotic kinesin KIF14 disrupts cell cycle progression and induces cytokinesis failure. Mol Cell Biol *26*, 3853-3863. 10.1128/MCB.26.10.3853-3863.2006.

S146. Zhu, C., Zhao, J., Bibikova, M., Leverson, J.D., Bossy-Wetzel, E., Fan, J.B., Abraham, R.T., and Jiang, W. (2005). Functional analysis of human microtubule-based motor proteins, the kinesins and dyneins, in mitosis/cytokinesis using RNA interference. Mol Biol Cell *16*, 3187-3199. 10.1091/mbc.e05-02-0167.

S147. Draviam, V.M., Stegmeier, F., Nalepa, G., Sowa, M.E., Chen, J., Liang, A., Hannon, G.J., Sorger, P.K., Harper, J.W., and Elledge, S.J. (2007). A functional genomic screen identifies a role for TAO1 kinase in spindle-checkpoint signalling. Nat Cell Biol *9*, 556-564. 10.1038/ncb1569.

S148. Shrestha, R.L., Tamura, N., Fries, A., Levin, N., Clark, J., and Draviam, V.M. (2014). TAO1 kinase maintains chromosomal stability by facilitating proper congression of chromosomes. Open Biol *4*, 130108. 10.1098/rsob.130108.

S149. Hashizume, C., Nakano, H., Yoshida, K., and Wong, R.W. (2010). Characterization of the role of the tumor marker Nup88 in mitosis. Mol Cancer *9*, 119. 1476-4598-9-119 [pii]

10.1186/1476-4598-9-119.

S150. Uematsu, K., Okumura, F., Tonogai, S., Joo-Okumura, A., Alemayehu, D.H., Nishikimi, A., Fukui, Y., Nakatsukasa, K., and Kamura, T. (2016). ASB7 regulates spindle dynamics and genome integrity by targeting DDA3 for proteasomal degradation. J Cell Biol *215*, 95-106. 10.1083/jcb.201603062.

S151. Jaramillo-Lambert, A., Hao, J., Xiao, H., Li, Y., Han, Z., and Zhu, W. (2013). Acidic nucleoplasmic DNA-binding protein (And-1) controls chromosome congression by regulating the assembly of centromere protein A (CENP-A) at centromeres. J Biol Chem *288*, 1480-1488. 10.1074/jbc.M112.429266.

S152. Zhu, M., Wang, F., Yan, F., Yao, P.Y., Du, J., Gao, X., Wang, X., Wu, Q., Ward, T., Li, J., et al. (2008). Septin 7 interacts with centromere-associated protein E and is required for its kinetochore localization. J Biol Chem *283*, 18916-18925. 10.1074/jbc.M710591200.

S153. Kim, S., and Jang, C.Y. (2016). ANKRD53 interacts with DDA3 and regulates chromosome integrity during mitosis. Biochem Biophys Res Commun *470*, 484-491. 10.1016/j.bbrc.2016.01.144.

S154. Milev, M.P., Hasaj, B., Saint-Dic, D., Snounou, S., Zhao, Q., and Sacher, M. (2015). TRAMM/TrappC12 plays a role in chromosome congression,

kinetochore stability, and CENP-E recruitment. The Journal of cell biology *209*, 221-234. 10.1083/jcb.201501090.

S155. Spiliotis, E.T., Kinoshita, M., and Nelson, W.J. (2005). A mitotic septin scaffold required for Mammalian chromosome congression and segregation. Science *307*, 1781-1785. 10.1126/science.1106823.

S156. Zuccolo, M., Alves, A., Galy, V., Bolhy, S., Formstecher, E., Racine, V., Sibarita, J.B., Fukagawa, T., Shiekhattar, R., Yen, T., and Doye, V. (2007). The human Nup107-160 nuclear pore subcomplex contributes to proper kinetochore functions. EMBO J *26*, 1853-1864. 10.1038/sj.emboj.7601642.

S157. Platani, M., Santarella-Mellwig, R., Posch, M., Walczak, R., Swedlow, J.R., and Mattaj, I.W. (2009). The Nup107-160 nucleoporin complex promotes mitotic events via control of the localization state of the chromosome passenger complex. Mol Biol Cell *20*, 5260-5275. 10.1091/mbc.E09-05-0377.

S158. Bancroft, J., Auckland, P., Samora, C.P., and McAinsh, A.D. (2015). Chromosome congression is promoted by CENP-Q- and CENP-E-dependent pathways. Journal of cell science *128*, 171-184. 10.1242/jcs.163659.

S159. Koliou, X., Fedonidis, C., Kalpachidou, T., and Mangoura, D. (2016). Nuclear import mechanism of neurofibromin for localization on the spindle and function in chromosome congression. J Neurochem *136*, 78-91. 10.1111/jnc.13401.

S160. Zhuo, X., Guo, X., Zhang, X., Jing, G., Wang, Y., Chen, Q., Jiang, Q., Liu, J., and Zhang, C. (2015). Usp16 regulates kinetochore localization of Plk1 to promote proper chromosome alignment in mitosis. J Cell Biol *210*, 727-735. 10.1083/jcb.201502044.

S161. Oh, H.J., Kim, M.J., Song, S.J., Kim, T., Lee, D., Kwon, S.H., Choi, E.J., and Lim, D.S. (2010). MST1 limits the kinase activity of aurora B to promote stable

kinetochore-microtubule attachment. Curr Biol *20*, 416-422. 10.1016/j.cub.2009.12.054.

S162. Shimizu, H., Nagamori, I., Yabuta, N., and Nojima, H. (2009). GAK, a regulator of clathrin-mediated membrane traffic, also controls centrosome integrity and chromosome congression. J Cell Sci *122*, 3145-3152. 10.1242/jcs.052795.

S163. Basilico, F., Maffini, S., Weir, J.R., Prumbaum, D., Rojas, A.M., Zimniak, T., De Antoni, A., Jeganathan, S., Voss, B., van Gerwen, S., et al. (2014). The pseudo GTPase CENP-M drives human kinetochore assembly. Elife *3*, e02978. 10.7554/eLife.02978.

S164. Foltz, D.R., Jansen, L.E., Black, B.E., Bailey, A.O., Yates, J.R., 3rd, and Cleveland, D.W. (2006). The human CENP-A centromeric nucleosome-associated complex. Nat Cell Biol *8*, 458-469. 10.1038/ncb1397.

S165. Hua, S., Wang, Z., Jiang, K., Huang, Y., Ward, T., Zhao, L., Dou, Z., and Yao, X. (2011). CENP-U cooperates with Hec1 to orchestrate kinetochore-microtubule attachment. J Biol Chem *286*, 1627-1638. 10.1074/jbc.M110.174946.

S166. He, J., Zhang, Z., Ouyang, M., Yang, F., Hao, H., Lamb, K.L., Yang, J., Yin, Y., and Shen, W.H. (2016). PTEN regulates EG5 to control spindle architecture and chromosome congression during mitosis. Nat Commun *7*, 12355. 10.1038/ncomms12355.

S167. O'Regan, L., Sampson, J., Richards, M.W., Knebel, A., Roth, D., Hood, F.E., Straube, A., Royle, S.J., Bayliss, R., and Fry, A.M. (2015). Hsp72 is targeted to the mitotic spindle by Nek6 to promote K-fiber assembly and mitotic progression. J Cell Biol *209*, 349-358. 10.1083/jcb.201409151.

S168. Serio, G., Margaria, V., Jensen, S., Oldani, A., Bartek, J., Bussolino, F., and Lanzetti, L. (2011). Small GTPase Rab5 participates in chromosome congression and regulates localization of the centromere-associated protein CENP-F to kinetochores. Proc Natl Acad Sci U S A *108*, 17337-17342. 10.1073/pnas.1103516108.

S169. Liu, S.T., Hittle, J.C., Jablonski, S.A., Campbell, M.S., Yoda, K., and Yen, T.J. (2003). Human CENP-I specifies localization of CENP-F, MAD1 and MAD2 to kinetochores and is essential for mitosis. Nat Cell Biol *5*, 341-345. 10.1038/ncb953.

S170. Nishihashi, A., Haraguchi, T., Hiraoka, Y., Ikemura, T., Regnier, V., Dodson, H., Earnshaw, W.C., and Fukagawa, T. (2002). CENP-I is essential for centromere function in vertebrate cells. Dev Cell *2*, 463-476. 10.1016/s1534-5807(02)00144-2.

S171. Kline, S.L., Cheeseman, I.M., Hori, T., Fukagawa, T., and Desai, A. (2006). The human Mis12 complex is required for kinetochore assembly and proper chromosome segregation. J Cell Biol *173*, 9-17. 10.1083/jcb.200509158.

S172. Lin, Y.T., Chen, Y., Wu, G., and Lee, W.H. (2006). Hec1 sequentially recruits Zwint-1 and ZW10 to kinetochores for faithful chromosome segregation and spindle checkpoint control. Oncogene *25*, 6901-6914. 10.1038/sj.onc.1209687.

S173. Wang, H., Hu, X., Ding, X., Dou, Z., Yang, Z., Shaw, A.W., Teng, M., Cleveland, D.W., Goldberg, M.L., Niu, L., and Yao, X. (2004). Human Zwint-1 specifies localization of Zeste White 10 to kinetochores and is essential for mitotic checkpoint signaling. J Biol Chem *279*, 54590-54598. 10.1074/jbc.M407588200.

S174. Ghongane, P., Kapanidou, M., Asghar, A., Elowe, S., and Bolanos-Garcia, V.M. (2014). The dynamic protein Knl1 - a kinetochore rendezvous. J Cell Sci *127*, 3415-3423. 10.1242/jcs.149922.

S175. Caldas, G.V., and DeLuca, J.G. (2014). KNL1: bringing order to the kinetochore. Chromosoma *123*, 169-181. 10.1007/s00412-013-0446-5.

S176. Mackay, D.R., Elgort, S.W., and Ullman, K.S. (2009). The nucleoporin Nup153 has separable roles in both early mitotic progression and the resolution of mitosis. Mol Biol Cell *20*, 1652-1660. 10.1091/mbc.E08-08-0883.

S177. Lussi, Y.C., Shumaker, D.K., Shimi, T., and Fahrenkrog, B. (2010). The nucleoporin Nup153 affects spindle checkpoint activity due to an association with Mad1. Nucleus *1*, 71-84. 10.4161/nucl.1.1.10244.

S178. Chatel, G., and Fahrenkrog, B. (2011). Nucleoporins: leaving the nuclear pore complex for a successful mitosis. Cell Signal *23*, 1555-1562. 10.1016/j.cellsig.2011.05.023.

S179. Honda, S., Marumoto, T., Hirota, T., Nitta, M., Arima, Y., Ogawa, M., and Saya, H. (2004). Activation of m-calpain is required for chromosome alignment on the metaphase plate during mitosis. J Biol Chem *279*, 10615-10623. 10.1074/jbc.M308841200.

S180. Asteriti, I.A., Giubettini, M., Lavia, P., and Guarguaglini, G. (2011). Aurora-A inactivation causes mitotic spindle pole fragmentation by unbalancing microtubule-generated forces. Mol Cancer *10*, 131. 10.1186/1476-4598-10-131.

S181. Karamysheva, Z., Diaz-Martinez, L.A., Crow, S.E., Li, B., and Yu, H. (2009). Multiple anaphase-promoting complex/cyclosome degrons mediate the

degradation of human Sgo1. J Biol Chem *284*, 1772-1780. 10.1074/jbc.M807083200.

S182. Labade, A.S., Karmodiya, K., and Sengupta, K. (2016). HOXA repression is mediated by nucleoporin Nup93 assisted by its interactors Nup188 and Nup205. Epigenetics Chromatin *9*, 54. 10.1186/s13072-016-0106-0.

S183. Kops, G.J., Kim, Y., Weaver, B.A., Mao, Y., McLeod, I., Yates, J.R., 3rd, Tagaya, M., and Cleveland, D.W. (2005). ZW10 links mitotic checkpoint signaling to the structural kinetochore. J Cell Biol *169*, 49-60. 10.1083/jcb.200411118.

S184. Chan, Y.W., Fava, L.L., Uldschmid, A., Schmitz, M.H., Gerlich, D.W., Nigg, E.A., and Santamaria, A. (2009). Mitotic control of kinetochore-associated dynein and spindle orientation by human Spindly. J Cell Biol *185*, 859-874. 10.1083/jcb.200812167.

S185. Thomas, G.E., Bandopadhyay, K., Sutradhar, S., Renjith, M.R., Singh, P., Gireesh, K.K., Simon, S., Badarudeen, B., Gupta, H., Banerjee, M., et al. (2016). EB1 regulates attachment of Ska1 with microtubules by forming extended structures on the microtubule lattice. Nat Commun *7*, 11665. 10.1038/ncomms11665.

S186. Fielding, A.B., Lim, S., Montgomery, K., Dobreva, I., and Dedhar, S. (2011). A critical role of integrin-linked kinase, ch-TOG and TACC3 in centrosome clustering in cancer cells. Oncogene *30*, 521-534. 10.1038/onc.2010.431.

S187. Srivastava, S., and Panda, D. (2018). A centrosomal protein STARD9 promotes microtubule stability and regulates spindle microtubule dynamics. Cell Cycle *17*, 2052-2068. 10.1080/15384101.2018.1513764.

S188. Vassilopoulos, S., Esk, C., Hoshino, S., Funke, B.H., Chen, C.Y., Plocik, A.M., Wright, W.E., Kucherlapati, R., and Brodsky, F.M. (2009). A role for the CHC22 clathrin heavy-chain isoform in human glucose metabolism. Science *324*, 1192-1196. 10.1126/science.1171529.

S189. Cheng, T.S., Hsiao, Y.L., Lin, C.C., Hsu, C.M., Chang, M.S., Lee, C.I., Yu, R.C., Huang, C.Y., Howng, S.L., and Hong, Y.R. (2007). hNinein is required for targeting spindle-associated protein Astrin to the centrosome during the S and G2 phases. Exp Cell Res *313*, 1710-1721. 10.1016/j.yexcr.2007.02.023.

S190. Kuang, P., Chen, Z., Wang, J., Liu, Z., Wang, J., Gao, J., and Shen, L. (2017). Characterization of Aurora A and Its Impact on the Effect of Cisplatin-Based Chemotherapy in Patients with Non-Small Cell Lung Cancer. Transl Oncol *10*, 367-377. 10.1016/j.tranon.2017.02.010.

S191. Kesisova, I.A., Nakos, K.C., Tsolou, A., Angelis, D., Lewis, J., Chatzaki, A., Agianian, B., Giannis, A., and Koffa, M.D. (2013). Tripolin A, a novel small-molecule inhibitor of aurora A kinase, reveals new regulation of HURP's distribution on microtubules. PLoS One *8*, e58485. 10.1371/journal.pone.0058485.

S192. Liu, D., Ding, X., Du, J., Cai, X., Huang, Y., Ward, T., Shaw, A., Yang, Y., Hu, R., Jin, C., and Yao, X. (2007). Human NUF2 interacts with centromere-associated protein E and is essential for a stable spindle microtubule-kinetochore attachment. J Biol Chem *282*, 21415-21424. 10.1074/jbc.M609026200.

S193. Chun, Y., Lee, M., Park, B., and Lee, S. (2013). CSN5/JAB1 interacts with the centromeric components CENP-T and CENP-W and regulates their

proteasome-mediated degradation. J Biol Chem *288*, 27208-27219. 10.1074/jbc.M113.469221.

S194. Kim, S., and Yu, H. (2015). Multiple assembly mechanisms anchor the KMN spindle checkpoint platform at human mitotic kinetochores. J Cell Biol *208*, 181-196. 10.1083/jcb.201407074.

S195. Tsang, Y.H., Han, X., Man, W.Y., Lee, N., and Poon, R.Y. (2012). Novel functions of the phosphatase SHP2 in the DNA replication and damage checkpoints. PLoS One *7*, e49943. 10.1371/journal.pone.0049943.

S196. Xu, H., Choe, C., Shin, S.H., Park, S.W., Kim, H.S., Jung, S.H., Yim, S.H., Kim, T.M., and Chung, Y.J. (2014). Silencing of KIF14 interferes with cell cycle progression and cytokinesis by blocking the p27(Kip1) ubiquitination pathway in hepatocellular carcinoma. Exp Mol Med *46*, e97. 10.1038/emm.2014.23.

S197. Bernad, R., van der Velde, H., Fornerod, M., and Pickersgill, H. (2004). Nup358/RanBP2 attaches to the nuclear pore complex via association with Nup88 and Nup214/CAN and plays a supporting role in CRM1-mediated nuclear protein export. Mol Cell Biol *24*, 2373-2384. 10.1128/MCB.24.6.2373-2384.2004.

S198. Zhu, W., Ukomadu, C., Jha, S., Senga, T., Dhar, S.K., Wohlschlegel, J.A., Nutt, L.K., Kornbluth, S., and Dutta, A. (2007). Mcm10 and And-1/CTF4 recruit DNA polymerase alpha to chromatin for initiation of DNA replication. Genes Dev *21*, 2288-2299. 10.1101/gad.1585607.

S199. Yoshizawa-Sugata, N., and Masai, H. (2009). Roles of human AND-1 in chromosome transactions in S phase. J Biol Chem *284*, 20718-20728. 10.1074/jbc.M806711200.

S200. Kremer, B.E., Haystead, T., and Macara, I.G. (2005). Mammalian septins regulate microtubule stability through interaction with the microtubule-binding protein MAP4. Mol Biol Cell *16*, 4648-4659. 10.1091/mbc.e05-03-0267.

S201. Park, H.J., Lee, S.J., Sohn, Y.B., Jin, H.S., Han, J.H., Kim, Y.B., Yim, H., and Jeong, S.Y. (2013). NF1 deficiency causes Bcl-xL upregulation in Schwann cells derived from neurofibromatosis type 1-associated malignant peripheral nerve sheath tumors. Int J Oncol *42*, 657-666. 10.3892/ijo.2012.1751.

S202. Qian, Y., Wang, B., Ma, A., Zhang, L., Xu, G., Ding, Q., Jing, T., Wu, L., Liu, Y., Yang, Z., and Liu, Y. (2016). USP16 Downregulation by Carboxyl-terminal Truncated HBx Promotes the Growth of Hepatocellular Carcinoma Cells. Sci Rep *6*, 33039. 10.1038/srep33039.

S203. Lee, D.W., Zhao, X., Zhang, F., Eisenberg, E., and Greene, L.E. (2005). Depletion of GAK/auxilin 2 inhibits receptor-mediated endocytosis and recruitment of both clathrin and clathrin adaptors. J Cell Sci *118*, 4311-4321. 10.1242/jcs.02548.

S204. Wu, H., Zhou, Y., Wu, H., Xu, L., Yan, Y., Tong, X., and Yan, H. (2021). CENPN Acts as a Novel Biomarker that Correlates With the Malignant Phenotypes of Glioma Cells. Front Genet *12*, 732376. 10.3389/fgene.2021.732376.

S205. Chan, Y.W., Jeyaprakash, A.A., Nigg, E.A., and Santamaria, A. (2012). Aurora B controls kinetochore-microtubule attachments by inhibiting Ska complex-KMN network interaction. J Cell Biol *196*, 563-571. 10.1083/jcb.201109001.

S206. Zhang, G., Lischetti, T., Hayward, D.G., and Nilsson, J. (2015). Distinct domains in Bub1 localize RZZ and BubR1 to kinetochores to regulate the checkpoint. Nat Commun *6*, 7162. 10.1038/ncomms8162.

S207. Goshima, G., Kiyomitsu, T., Yoda, K., and Yanagida, M. (2003). Human centromere chromatin protein hMis12, essential for equal segregation, is independent of CENP-A loading pathway. The Journal of cell biology *160*, 25-39. 10.1083/jcb.200210005.

S208. Schleicher, K., Porter, M., Ten Have, S., Sundaramoorthy, R., Porter, I.M., and Swedlow, J.R. (2017). The Ndc80 complex targets Bod1 to human mitotic kinetochores. Open Biol *7*. 10.1098/rsob.170099.

S209. Hahn, P., Schmidt, C., Weber, M., Kang, J., and Bielke, W. (2004). RNA interference: PCR strategies for the quantification of stable degradation-fragments derived from siRNA-targeted mRNAs. Biomol Eng *21*, 113-117. 10.1016/j.bioeng.2004.09.001.